NASA Technical Memorandum 84378

Parabolized Navier-Stokes Solutions of Separation and Trailing-Edge Flows

James L. Brown

June 1983

NASA
National Aeronautics and
Space Administration

NASA Technical Memorandum 84378

Parabolized Navier-Stokes Solutions of Separation and Trailing-Edge Flows

James L. Brown, Ames Research Center, Moffett Field, California

National Aeronautics and
Space Administration

Ames Research Center
Moffett Field, California 94035

PARABOLIZED NAVIER-STOKES SOLUTIONS

of

SEPARATION and TRAILING-EDGE FLOWS

James L. Brown

Ames Research Center

SUMMARY

A robust, iterative solution procedure is presented for the parabolized Navier-Stokes or higher-order boundary-layer equations as applied to subsonic viscous-inviscid interaction flows. The robustness of the present procedure is due, in part, to an improved algorithmic formulation. The present formulation is based on a re-interpretation of stability requirements for this class of algorithms and requires only second-order-accurate backward or central differences for all streamwise derivatives. Upstream influence is provided for through the algorithmic formulation and iterative sweeps in x. The primary contribution to robustness, however, is the boundary-condition treatment, which imposes global constraints to control the convergence path. Discussed are successful calculations of subsonic, strong viscous-inviscid interactions, including separation. These results are consistent with Navier-Stokes solutions and triple-deck theory.

SYMBOLS

C_f	skin friction coefficient, $2\tau/\rho_e u_e^2$
C_p	pressure coefficient
e	total energy per unit mass, m^2/sec^2
$\dot{m}$	mass-flow rate, kg/sec
p	static pressure, $kg/m \cdot sec^2$
R	radius of curvature, m
Re_L	Reynolds number, uL/ν
u	velocity, x-component, m/sec
v	velocity, y-component, m/sec
x	Cartesian coordinate, m
y	Cartesian coordinate, m
δ^*	displacement thickness, m
η	transformed coordinate, $\eta = \eta(x, y)$
μ	dynamic viscosity, $kg/m \cdot sec$
ν	kinematic viscosity, m^2/sec
ξ	transformed coordinate, $\xi = x$
ρ	density, kg/m^3
τ	shear stress, $\mu \partial u/\partial y$
Ψ	streamfunction, $\int \rho u \, \delta y$

Subscripts:

CL	wake centerline value
e	edge value
i	grid index in x
j	grid index in y
TE	trailing-edge value
w	wall value

Superscript:

n	iteration level index

INTRODUCTION

Aerodynamic flows often involve physical phenomena not properly accounted for in first-order boundary-layer theory (ref. 1), even when coupled to an outer inviscid solution. For strong viscous-inviscid regions, such as the trailing-edge of an airfoil, or in a shock/boundary-layer interaction, streamline curvature leads to a significant normal pressure gradient $\partial p/\partial y$ within the boundary layer. Additionally, upstream effects may become important even within the thin viscous shear layer. Separation may also occur, further complicating the solution within these flow regions.

Some coupled methods (refs. 2-4) modify the results of their boundary-layer solutions within such regions in an attempt to correct for these deficiencies of first-order boundary-layer theory. However, the appropiateness of these corrections, valid only to first order, clouds related issues, such as turbulence modeling, within these regions. To resort to the time-dependent Navier-Stokes approach for these regions seems a needlessly expensive way of accounting for the weak ellipticity of these flows. Problems with grid resolution are also encountered in the application of time-dependent Navier-Stokes methods owing to storage and CFL condition limitations, even for the implicit methods prevalent (ref. 5). The present work addresses this clear need for an efficient viscous-solution method, one that is intermediate between currently available first-order boundary-layer and Navier-Stokes techniques, is capable of treating upstream influence and small-scale separation, and is suitable for viscous-inviscid coupling.

Previous workers have formulated sophisticated schemes with various regimes of applicability to solve viscous layers with higher-order effects. Here we concentrate on spatially marching schemes because of their implied promise of minimizing both storage requirements and convergence times while retaining the capability of treating complex geometries. Parabolized Navier-Stokes (PNS) methods have demonstrated considerable success when applied to supersonic flow over complex bodies. The most prevalent PNS methods (refs. 6,7) currently are single-sweep, noniterative and are faster than time-dependent Navier-Stokes solvers by orders of magnitude, thus

making three-dimensional computations quite practical. Such PNS methods effectively solve the continuity, x-momentum, y-momentum, and energy equations for ρ, ρu, ρv, and ρe, respectively. Pressure is obtained from the equation of state. Currently, such PNS solvers are restricted to supersonic flows with thin subsonic regions. The treatment of the pressure terms within the subsonic regions is only approximate but is critical to obtain stable marching. For stable marching, a minimum streamwise step $\Delta x \geq \Delta x_{min}$ must be taken. This minimum step size is roughly the height of the subsonic region. Axial separation is not allowed. These PNS methods currently involve only single sweeps in the x-direction and thus cannot provide for upstream influence.

Partially-parabolized Navier-Stokes (PPNS) methods provide solutions for large regions of subsonic and even reversed flow. In these methods (refs. 8,9), the x- and y- momentum equations are spatially marched with the pressure field assumed known. The continuity equation is then used as a basis for corrections to the pressure field. Some PPNS methods also solve an elliptic Poisson equation which aids in transmitting pressure information throughout the entire flow field, but also adds to the computational time and effort. The specification of u and v boundary conditions does not easily fit into current coupling schemes. Upstream influence is possible with these methods and multiple sweeps in the x-direction are necessary.

More suited to application in a viscous-inviscid coupling scheme are PNS methods that are essentially boundary-layer methods with incorporation of the y-momentum equation. Incorporation of the y-momentum equation elevates the conventional first-order boundary-layer equations into the PNS set of equations. Upstream influence is provided through multiple-sweeps in the x-direction and through proper design of the algorithm. Primary contributions to these methods were made by Rubin (ref. 10), Lin and Rubin (ref. 11), Maghoub and Bradshaw (ref. 12), and Chen and Bradshaw (ref. 13). These PNS methods effectively solve the continuity, x-momentum, y-momentum and energy equations for v, u, p, and ρe respectively. The equation of state is used to solve for ρ. For incompressible flows, the variable ρe and the energy equation may be dropped.

Rubin applied such a PNS/boundary-layer method to an incompres-

sible separation problem. The method is implicit with the equations coupled. Rubin emphasized forward-differencing of $\partial p/\partial x$ inconsistent with the differencing treatment of the remaining streamwise derivatives as a requirement for stable marching. Extension to compressible flows was accomplished by Lin and Rubin in a study of supersonic viscous flow over an inclined cone. This class of flows contains negligible upstream influence and is efficiently solved by the single-sweep PNS methods. Convergence of their multiple-sweep PNS/boundary-layer method did occur, albeit slowly. Rubin and Reddy (ref. 14) subsequently applied a multigrid technique to aid convergence and robustness on fine grids.

Chen and Bradshaw presented an efficient viscous-inviscid coupling scheme based on the PNS/boundary-layer method of Maghoub and Bradshaw which includes the y-momentum equation. Good agreement of the calculations with experimental C_p versus x was obtained for two airfoils at transonic speeds but at a small angle of attack. The boundary-layer equations are solved uncoupled, and it would appear that the technique, being based on the method of characteristics, cannot calculate through flow-reversal. Chen and Bradshaw concede that if $\partial^2 p/\partial x \partial y$ is significant their method may fail.

Both of the above higher-order boundary-layer methods are significant contributions. Both of these methods, however, have limitations as to accuracy and robustness. Accuracy is limited in both methods since forward-differencing of $\partial p/\partial x$ is used in the x-momentum equation for stability and upstream influence, and backward-differencing is used for all other x-derivatives. As a model equation, even the differential form of the Bernoulli equation will be solved inaccurately.

In this paper, the requirement of forward-differencing of $\partial p/\partial x$ for stability and upstream influence is removed. A consistent algorithm is formulated, thereby improving the inherent accuracy of this class of methods. Coarser grids are allowed which aids the convergence rate, and the robustness of the current method is considerably enhanced relative to the prior methods, a result of both the $\partial p/\partial x$ and boundary-condition treatments.

The method in this paper is an implicit, finite-difference solution of the PNS or higher-order boundary-layer approximation of the Navier-Stokes

equations. In addition to the continuity and x-momentum equations solved by first-order boundary-layer techniques, inclusion of the y-momentum equation is accomplished. Inclusion of the y-momentum equation allows for solution with normal pressure gradients but converts the parabolic first-order boundary-layer equations into an elliptic set. This is demonstrated by dropping the viscous terms, thereby obtaining the Euler equations as a subset. An otherwise parabolic spatially marching procedure is rendered elliptic by providing for upstream propagation of information relating to the pressure field. Second-order-accurate backward or central differences are used for the streamwise derivatives, leading to an accurate and consistent scheme. Physical insight allows the x- and y- momentum equations to be written in a form so that the scheme is also stable. Iterative sweeps in the x-direction are required with global storage for only pressure being neccessary. The only special treatment required for separation is to set $\rho u \partial u/\partial x = 0$ in the x-momentum equation.

The boundary conditions of the method presented here are similar to those of conventional first-order boundary-layer methods with either a direct edge-pressure, or an inverse mode. Efficient algorithms exist for coupling with an inviscid code, using either the direct or the inverse boundary conditions. The boundary conditions implemented are thus well-suited for incorporation of the method into a coupled viscous-inviscid procedure. The psuedodirect boundary condition is actually an adaption of a proposed semi-inverse coupling procedure. For duct flow, where mass flow remains constant, the present code can proceed to a solution without the neccessity of coupling. The influence of the type of boundary condition used on convergence is observed and discussed. To validate the method, results are presented for a variety of flow conditions. Comparisons are made with available Navier-Stokes solutions and triple-deck theory.

NUMERICAL FORMULATION

The equations that are solved for incompressible, two-dimensional flows are

$$\begin{aligned} \frac{\partial u}{\partial x} + \frac{\partial v}{\partial y} &= 0 \\ c\rho u\frac{\partial u}{\partial x} + \rho v\frac{\partial u}{\partial y} &= -\frac{\partial p}{\partial x} + \frac{\partial}{\partial y}\left\{\mu\frac{\partial u}{\partial y}\right\} \\ \rho u\frac{\partial v}{\partial x} + \rho v\frac{\partial v}{\partial y} &= -\frac{\partial p}{\partial y} \end{aligned} \tag{1}$$

where the FLARE approximation (ref. 15) is used

$$\begin{aligned} c &= 1 \quad if\ u \geq 0 \\ &= 0 \quad if\ u < 0 \end{aligned}$$

Boundary conditions are discussed later.

For coupled systems of equations, a variable that is being solved for may be associated with a particular equation through diagonal dominance of the resultant matrix system. As with conventional first-order boundary-layer techniques, the solution for u and v is associated with the x-momentum and continuity equations, respectively. The solution for pressure is associated with the y-momentum equation. In contrast, PPNS methods solve for u and v from the x- and y- momentum equations, respectively. This difference is not just a subtle point. Not only are simpler boundary condition specifications required in the present formulation, but also the pressure field is being solved in an implicit coupled fashion simultaneously with the velocity field. In PPNS methods, the pressure-field calculations are decoupled and are lagged relative to the velocity-field calculations. Generally speaking, methods that are implicit and fully coupled are more robust and converge faster than methods that are not.

One key idea in the present formulation is that in deriving the finite-difference representation of the above differential equations, no equation is written at the same location. By so doing, stable marching is achieved while also arriving at a sparse block-tridiagonal matrix system which may be more economically solved. Figure 1 depicts the various nodes involved in writing

the finite-difference equations. In figure 1, the equation is written formally at $(i, j\text{-}1/2)$ for continuity; (i, j) for x-momentum; and $(i\text{-}1, j + 1/2)$ for y-momentum. In marching the solution one streamwise step, the variables u and v are being solved for at x_i, and p is being solved for at x_{i-1}. The continuity and x-momentum equations use backward differences for the x-derivatives. The backward-difference expression for the $\partial p/\partial x$ term with evenly-spaced Δx is

$$\frac{\partial p}{\partial x}\Big|_{i,j}^{n} = \frac{3p_{i,j}^{n-1} - 4p_{i-1,j}^{n} + p_{i-2,j}^{n}}{2\Delta x} \tag{2}$$

The superscript n refers to the global iteration level. Note that $p_{i-2,j}^{n}$ has been solved for, $p_{i-1,j}^{n}$ is being simultaneously solved for from the y-momentum equation, and $p_{i,j}^{n-1}$ must be obtained from a previous global iteration. Upstream values of v^n at x_i are involved in the y-momentum solution for p^n at x_{i-1}. Upstream influence is thus provided for through the (y-momentum and $\partial p/\partial x$) pressure formulation. Were the y-momentum equation to be written at x_i, not only would the upstream propagation of pressure information be suppressed, but the scheme would be unstable for small Δx.

The metric treatment used allows more general body shapes than does a rectangular grid, while minimizing the complexity involved during the early phases of code development. Consider the rather simple metric transformation

$$\begin{aligned} x &= \xi; \quad y = y(\xi, \eta) \\ \xi &= x; \quad \eta = \eta(x, y) = j \end{aligned} \tag{3}$$

The x- and y- derivatives may be written as

$$\begin{aligned} \frac{\partial}{\partial x} &= \frac{\partial \eta}{\partial x}\frac{\partial}{\partial \eta} + \frac{\partial}{\partial \xi} \\ \frac{\partial}{\partial y} &= \frac{\partial \eta}{\partial y}\frac{\partial}{\partial \eta} \end{aligned} \tag{4}$$

The term $\partial \eta/\partial x$ can be written for the above transformation as

$$\frac{\partial \eta}{\partial x} = -\frac{\partial \eta}{\partial y}\frac{\partial y}{\partial \xi} \tag{5}$$

which leads to

$$\frac{\partial}{\partial x} = \frac{\partial}{\partial \xi} - \frac{\partial y}{\partial \xi}\frac{\partial}{\partial y}; \quad \frac{\partial y}{\partial \xi} = \frac{y_{i,j} - y_{i-1,j}}{\xi_i - \xi_{i-1}} \tag{6}$$

The x-derivatives in the differential system, equation 1, are then written using equation 6, and the y-derivatives are written as y-derivatives using higher-order-accurate numerical forms for variable grid spacing. The solution then actually occurs in a hybrid ξ, y system. Metric treatments of the type presented by Steger (ref. 16) are contemplated for future incorporation; however, a quite wide range of problems with interesting geometries may be studied with the metric treatment described.

Using the above metrics, second-order-accurate finite differences, and the finite-difference molecule depicted in figure 1, the differential system given by equation 1 can be written in matrix form

$$(A_{k,m})_j(U_m)_{j-1} + (B_{k,m})_j(U_m)_j + (C_{k,m})_j(U_m)_{j+1} = (D_k)_j \tag{7}$$

where

j =1, $jmax$ refers to the jth differencing molecule(see fig.1)

k refers to the equation:

=1, continuity

=2, x-momentum

=3, y-momentum

m refers to the variable:

=1, $(U_1)_j \equiv \Delta v_{i,j} = v_{i,j} - v_{i-1,j}$

=2, $(U_2)_j \equiv \Delta u_{i,j} = u_{i,j} - u_{i-1,j}$

=3, $(U_3)_j \equiv p_{i-1,j}$

The interior elements for matrices A,B,C, and D are given in the appendix. This matrix system is then solved using a standard 3 x 3 block-tridiagonal matrix solver rewritten to take advantage of the matrix sparsity. The sparsity of the matrix system is depicted in figure 2. The convective coefficients, $(\rho u)_{i,j}$ and $(\rho v)_{i,j}$, appearing in the x-momentum equation involve unknowns being solved for. Iteration for these coefficients makes

the finite-difference approximation to the differential system second-order-accurate. Typically, three iterations are used with the values at $(i\text{-}1, j)$ used in the first iteration. Extrapolation for these coefficients was tried; however, the converged solutions for separated flows exhibited weak spatial oscillations. Note that the y-momentum equation is solved for at $(i\text{-}1, j + 1/2)$; therefore, these convective coefficients are known.

A computer code written in FORTRAN implements the above algorithm for two-dimensional steady, incompressible laminar flows. The code operates in either a PNS or a first-order boundary-layer (BL, where $\partial p/\partial y \equiv 0$ replaces the y-momentum equation) option. Such an ability to easily choose between the PNS and BL formulations allows accurate evaluation of the significance of the y-momentum equation for various flow conditions. Several boundary-condition options are implemented. These are next described.

The boundary conditions for a solid surface are

$$\begin{aligned} \text{continuity at } x_i : v_{i,1} &= 0 \text{ at wall} \\ x\text{-momentum at } x_i : u_{i,1} &= 0 \text{ at wall} \\ \frac{\partial u}{\partial y} &= 0 \text{ at edge} \end{aligned} \tag{8}$$

An additional edge condition is required for the y-momentum equation on the pressure. The treatment of this additional edge condition leads to four boundary-condition options: the direct mode, duct mode, inverse mode, and psuedodirect mode.

Direct mode – The direct mode applies an input pressure distribution $p_{i,jmax}$ versus x_i as an edge condition to the y-momentum equation. This option is referred to as the PNS-Direct or the BL-Direct mode depending on whether the PNS or the BL option is in effect.

Duct mode – The duct mode applies a correction to the overall pressure level at x_i to maintain a constant mass flow, $\dot{m}$, through the duct. The value of $\dot{m}$ is obtained from the inlet profile at x_1. With $p^{n-1}_{i,j}$, $p^{n}_{i-1,jmax}$, and PC^{n}_{i-1} assumed known, the following FORTRAN assignment statements are used:

$$
\begin{aligned}
p^{n-1}_{i,j} &= p^{n-1}_{i,j} + PC^n_i \\
&\quad (\text{ used in the } \frac{\partial p}{\partial x} \; x\text{-momentum equation term}) \\
p^n_{i-1,jmax} &= p^{n-1}_{i-1,jmax} + PC^n_{i-1} \\
&\quad (\text{ used as the } y\text{-momentum equation edge condition})
\end{aligned} \tag{9}
$$

The pressure level correction, PC^n_i, is found by iteration through a modified secant method relating $\dot{m}_i$ to PC^n_i. Typically three or four iterations are required. This option is referred to as the PNS-Duct or BL-Duct mode.

Inverse mode – The inverse mode is similar to the duct mode except that the pressure correction being applied is adjusted so that an input edge streamfunction is obtained, $\Psi_{e,i}$ versus x_i where

$$
\Psi_{e,i} \equiv \int_{y_w}^{y_e} u \, \delta y \tag{10}
$$

This inverse mode is similar to the more conventional δ^*-specified inverse mode. Note that Ψ_e and δ^* are related by

$$
\Psi_e = u_e(y_e - y_w - \delta^*) \tag{11}
$$

This option is referred to as the PNS-INV or BL-INV mode.

Psuedodirect mode – The psuedodirect mode is similar to the inverse mode except that the edge streamfunction distribution $\Psi_{e,i}$ versus x_i is adjusted every global iteration. The adjustment is accomplished to give, upon convergence, a desired edge-velocity distribution; it is based on a coupling algorithm that is being explored. The algorithm used is

$$
\Psi^n_e = \Psi^{n-1}_e + \frac{\delta \Psi_e}{\delta u_e} \Delta u_e \tag{12}
$$

where

$$
\frac{\delta \Psi_e}{\delta u_e} = (y_e - y_w - \delta^*) - u_e \frac{\delta \delta^*}{\delta u_e} = \frac{\Psi^{n-1}_e}{u^{n-1}_e} - u_e \frac{\delta \delta^*}{\delta u_e} \tag{13}
$$

Since $\delta\delta^*/\delta u_e$ is not easily evaluated, this term is at present dropped and underrelaxation is used giving

$$\Psi_e^n = \Psi_e^{n-1} + C\frac{\Psi_e^{n-1}}{u_e^{n-1}}\Delta u_e \tag{14}$$

Here Δu_e is the difference between the desired edge velocity at x_i and the edge velocity u_e^{n-1} from the last global iteration. The desired edge velocity can be either an input edge-velocity distribution, as with the present psuedodirect mode, or can be an edge-velocity distribution obtained from an inviscid solver, as in a viscous-inviscid coupling procedure. A similarity exists to Carter's δ^* semi-inverse algorithm (ref. 17)

$$\delta^{*n} = \delta^{*n-1}\frac{u_{e,viscous}^{n-1}}{u_{e,inviscid}^{n-1}} \tag{15}$$

The psuedodirect option demonstrates the essential features of the coupling algorithm and accelerates convergence over the direct mode for the specified edge-velocity boundary condition. The psuedodirect mode is used only with the PNS option and is referred to as the PNS-PSD mode. The logic for the PNS-PSD mode is demonstrated in block form in figure 3.

For the symmetric wake, the boundary condition for the x-momentum equation differs at $y = 0$. The symmetry of u about $y = 0$ is made use of to evaluate the x-momentum equation at $y = 0$ as

$$(\rho u)_{i,1}^n \frac{\partial u}{\partial x}\Big|_{i,1}^n = -\frac{\partial p}{\partial x}\Big|_{i,1}^n + 2\mu_{i,1+1/2}^n \frac{(u_{i,2}^n - u_{i,1}^n)}{(y_{i,2} - y_{i,1})^2} \tag{16}$$

The $\partial/\partial x$ terms are expanded as before. The symmetric wake boundary condition above is second-order accurate and gives a smoother representation of the inner wake than does the first-order $\partial u/\partial y = 0$ condition normally applied.

RESULTS

The method described in the previous sections was applied to several laminar flows that involve strong viscous-inviscid interactions. These flows included the Briley laminar separation cases and the symmetric laminar wake of a flat plate. Much of the development work on the algorithm and boundary-condition treatments was accomplished while considering the Briley separation cases.

Laminar Separation Results

Briley (ref. 18) solved the time-dependent Navier-Stokes equations over a flat plate for a set of four linearly retarded flows. The edge velocity is prescribed at $y_e = 3.81 \times 10^{-3}$ m for these four flows as

$$\begin{aligned} u_e(\text{m/sec}) &= 30.48(1 - 3x) \,, \; x \leq x_c \\ &= C \qquad\qquad\quad \,, \; x > x_c \end{aligned} \tag{17}$$

The four Briley cases differ in the location x_c and velocity level C. Briley faired the curve at x_c to avoid a discontinuity in slope. The kinematic viscosity is $\nu = 1.4864 \times 10^{-4}$ m^2/sec. The specification of these parameters by Briley was in English units (the nondimensional Reynolds number being the important constant) and have been subsequently converted to metric for this study. Two of the four Briley cases (Briley-1 and -2) are attached flows; the other two (Briley-3 and -4) exhibit separation bubbles of differing extent. Elliptic or upstream effects are significant in these flows and, in contrast, a pressure-prescribed first-order boundary-layer solution (Howarth flow) predicts separation for all four cases. Since the geometry of these cases is simple, and separation with upstream influence does occur, these flows have been used in various studies as standard test cases for validating and developing new numerical algorithms for calculations in fluid mechanics.

The initial efforts at solving the Briley cases made use of an algorithm quite similar to that of Rubin, in that forward-differencing of $\partial p/\partial x$ and backward-differencing of $\partial u/\partial x$ were implemented in the x-momentum

equations. Coarse-grid solutions inevitably did not separate since the adverse pressure gradient was being relieved prematurely owing to the use of a forward-differenced $\partial p/\partial x$. Fine-grid solutions could be obtained with underrelaxation but the method lacked robustness. It was realized during these initial efforts that for these methods to be generally and routinely applicable for industrial and aerodynamic design purposes, developments had to be made to

1. Eliminate the inconsistent use of forward-differenced $\partial p/\partial x$ and backward-differenced $\partial u/\partial x$ in the x-momentum equation

2. Enhance accuracy on coarse grids

3. Enhance robustness, particularly when applied to flows with severe adverse pressure gradients

4. Promote rapid convergence

An important development was the realization, based partly on physical arguments, that stable marching of this class of algorithms requires that the pressure variable solved for be the trailing pressure (with a dominant negative coefficient) in the $\partial p/\partial x$ term; Rubin's stability requirement of forward-differencing for the $\partial p/\partial x$ term is unneccessarily restrictive. Solving for the trailing pressure leads to damping of error terms, whereas solving for the leading pressure leads to error amplification and the associated departure solutions described by Lighthill (ref. 19). Subsequently, the present fully implicit algorithm was formulated with second-order-accurate backward-differenced $\partial\,/\partial x$ used exclusively for the continuity and the x-momentum equations, and second-order-accurate central-differenced $\partial\,/\partial x$ used for the y-momentum equation. Improvements in accuracy and robustness were demonstrated by the elimination of the forward-differenced $\partial p/\partial x$. The convergence rate was, however, still felt to be slower for the Briley flows than one might reasonably expect. The development of a plot package depicting streamline and pressure contours revealed intermediate solutions with substantial streamline curvature, which in some cases verged on being physically unrealistic. At this point, a decision was made to develop a treatment of the boundary conditions that would more affirmatively control the convergence path of these intermediate solutions. This led to the PNS-INV and later to the PNS-PSD boundary-condition modes.

The Briley-3 separated-flow case was selected for more intensive study instead of the Briley-4 case because of limitations of the PNS-Direct mode. Also, various Navier-Stokes methods give somewhat different solutions for the Briley-4 case since significant viscous effects extend to the edge of the computational domain, and details of boundary-condition treatment acquire importance. Fully converged solutions for the Briley-4 case were obtained with the PNS-PSD mode, however. Thus, the attached Briley-1 and the separated Briley-3 cases were chosen for use in the present study for validation purposes. Five modes of operation of the present code were applied to the Briley-3 and -1 cases: (1) PNS-Direct; (2) PNS-INV; (3) PNS-PSD; (4) BL-Direct; and (5) BL-INV. Coarse- and fine-grid solutions were obtained. The Briley-3 case is discussed first.

Briley-3 case – Figure 4 depicts the edge-velocity distribution used for the Briley-3 case as the input boundary condition for the PNS-Direct and PNS-PSD modes. The position for separation as given by the Briley Navier-Stokes and by the first-order boundary-layer (Howarth flow) solutions are marked; reattachment as calculated by Briley is indicated as well. Murphy (ref. 20) demonstrated that the difference between the Navier-Stokes and first-order boundary-layer separation points is a function of the Reynolds number of the flow, with agreement occurring at sufficiently high Reynolds number. For the PNS-INV and BL-INV modes the input boundary condition used was the edge streamfunction calculated from the PNS-PSD mode. The output result for the inverse modes is a calculated edge-velocity distribution. The resultant edge-velocity distribution from the PNS-INV mode is identical with the input distribution to the PNS-PSD mode, as one might reasonably expect. The BL-INV mode, however, gives an edge-velocity distribution in which the greatest differences occur in the region of the separation bubble, where $\partial p/\partial y \not\equiv 0$ effects are most significant.

The streamline and pressure contours obtained for the PNS-INV mode are combined in figure 5. The PNS-PSD solution is essentially identical. The streamlines are not evenly spaced, being more tightly spaced close to the surface to provide more detail. The pressure contours are evenly spaced in pressure. The x-spacing of the pressure contours gives an indication of the streamwise pressure gradient, and the slope of a particular pressure

contour is inversely related to the normal pressure gradient:

$$\frac{\partial p}{\partial y}|_x = -\frac{\partial p}{\partial x}|_y \Big/ \frac{\partial y}{\partial x}|_p \tag{18}$$

A fine-grid (36 x-stations) solution is shown. Minor differences in streamlines for the coarse-grid (18 x-stations) solution exist, but are not significant. For most purposes, the accuracy of the coarse-grid 10th iteration solution would suffice. Thus, rapid convergence to an accurate solution is demonstrated on a coarse grid for the current algorithm with the PNS-INV boundary-condition mode.

The combined streamline and pressure-contour plot makes it possible to gain insight into both the flow being computed and the algorithm employed. One connection between the pressure field and streamlines is through the y-momentum equation, rewritten here as

$$\frac{\partial p}{\partial y} = -\frac{\rho u^2}{R}; \quad \frac{1}{R} \equiv \frac{\partial (v/u)}{\partial x} \tag{19}$$

where R is interpreted as the radius of curvature of the local streamline. Were R to be interpreted as the surface curvature, as in some boundary-layer methods, the ellipticity of the present method would be suppressed. Note that close to the surface within δ^*, even though the streamline curvature is substantial, the normal pressure gradient is nearly zero. This is, of course, because the ρu^2 term is quite small. Only in the inviscid region and in the viscous region outside δ^* do strong $\partial p/\partial y$ effects occur, being most significant for those x-stations in the vicinity of the separation bubble, where streamline curvature is large. In the vicinity of the separation point, the streamline curvature and associated $\partial p/\partial y$ effects tend to relieve the surface-pressure gradient ($\partial p/\partial x$) relative to the edge-pressure gradient, thereby delaying separation relative to a first-order boundary-layer solution. The weak adverse pressure gradient is, however, prolonged at the surface, thereby delaying reattachment till well past the x-station where the edge-pressure gradient is relieved. It is interesting to note that reattachment occurs in the presence of a weak adverse pressure gradient at the surface. Reattachment is apparently accomplished by the shear-stress transport of

momentum from the outer regions predominating over the weak residual adverse pressure gradient.

The considerable advantage in convergence rate of the PNS-INV mode over that of the PNS-Direct mode can best be understood in terms of this interaction between the pressure field and the streamline contours. With the edge streamline specified, the streamlines within the computational domain approximate fairly well the streamlines for the final converged solution, even on the first global iteration. The $\partial p/\partial y$ field establishes itself rather quickly in the global iteration process. For the PNS-Direct mode, the streamlines within the computational domain are not so constrained, and, particularly for separated flows, the initial streamlines differ markedly from the final converged solution; there is slower establishment of the pressure field, with slower overall convergence.

Figure 6 shows velocity profiles u versus y obtained using the PNS-PSD mode. In the interest of clarity, not all x-locations are presented. It is obvious that the velocity levels in the reversed-flow region are quite small, thereby justifying the FLARE approximation used in the present study. It is also apparent that the viscous region approaches but does not quite reach the edge of the computational domain for this Briley-3 case. Also observe that the outflow profile is Blasius in shape, in agreement with Briley. As indicated in figure 6, a stretched y-spacing is used, with 14 of 40 nodes adequate to resolve the inlet boundary layer. Solutions with even spacing in y give nearly the same result.

Figure 7 presents the distribution of skin friction C_f versus x and displacement thickness δ^* versus x calculated by the PNS-INV (identical to the PNS-PSD solution) and the BL-INV modes. Also given are the corresponding results from Briley's calculations. The skin-friction results indicate that the PNS-INV mode and Briley calculations agree identically with respect to reattachment location, with the PNS-INV mode giving separation one-half grid point farther downstream. The BL-INV mode gives surprisingly good agreement with Briley's separation point, with reattachment occcurring two grid points upstream of the Briley calculation results. Good agreement for the δ^* distribution exists for the PNS-INV and the Briley solutions. The BL-INV method once again demonstrates some differences for C_f and δ^*

in the region of significant $\partial p/\partial y$. The BL-INV method used appears to be a particularly attractive calculation method in view of the single global sweep required. Pletcher (ref. 21) has reached similar conclusions concerning an inverse BL, δ^*-prescribed, finite-difference method. An error in edge velocity in regions of significant $\partial p/\partial y$ inevitably occurs, however, with these inverse BL methods.

For the Briley-3 case, the PNS-PSD and PNS-INV modes give results quite comparable to the Navier-Stokes solutions by Briley. These methods converge rapidly, with about 20 global iterations required for the fine-grid PNS-INV solution and 10 global iterations for the coarse-grid PNS-INV solution. The iterations required for the PNS-PSD mode depend on the initial Ψ_e distribution. Using an initial distribution deduced from the Briley results, the fine-grid PNS-PSD converges in 40 global iterations. Here convergence is indicated when no significant changes occur in C_f, δ^*, or u_e. The pressure residual for these two methods goes to essentially machine zero. The PNS-Direct mode was also applied to the Briley-3 case with results similar to those of the PNS-PSD mode. The convergence characteristics are not as desirable, with the maximum pressure residual leveling off before reaching machine zero. For separated flows, the PNS-PSD mode exhibits considerable advantage over the PNS-Direct mode with respect to the convergence rate and robustness.

Briley-1 case – The Briley-1 attached-flow case was also calculated by the PNS and BL methods. Figure 8 indicates the edge-velocity distribution u_e versus x specified by Briley for this case. This u_e distribution is similar to that for the Briley-3 case but the adverse pressure gradient is not sustained for as long. Navier-Stokes solutions do not separate, even though separation is indicated by first-order boundary-layer theory (Howarth solution). Thus, upstream influence is significant for this flow. The skin-friction and displacement thickness results are shown in figure 9. The PNS-Direct, PNS-INV, and PNS-PSD modes all give results in agreement with the Navier-Stokes solutions of Briley. Once again, the BL-INV mode gives quite acceptable results with the greatest discrepancy occurring in regions of significant $\partial p/\partial y$. Also indicated are BL-Direct solutions for this case in the region leading to separation. The separation point indicated by the BL-Direct

results is in good agreement with the Howarth separation point. It is interesting to note that with the FLARE approximation being used, the BL-Direct mode will march through separation and reattachment. The solutions past separation are highly nonphysical, however, with a tremendous ejection of material upward from the separation point (see the discussion of Landau and Lifshitz (ref. 22) regarding the singularity at separation of the first-order boundary-layer equations). The substantial streamline curvature in the BL-Direct solutions close to separation is at considerable variance with the first-order boundary-layer theory assumption of $\partial p/\partial y \equiv 0$.

Trailing Edge Results

The laminar, flat-plate trailing-edge provides a further example of the applicability of the present PNS formulation to strong viscous-inviscid interactions. In the absence of upstream influence, a simple discontinuity in boundary condition occurs for first-order boundary-layer theory at the trailing-edge. Goldstein (ref. 23) provides such first-order boundary-layer solutions for the trailing-edge/near-wake problem. However, for the Navier-Stokes equations and equation subsets which properly account for upstream influence, the laminar trailing-edge problem contains a singularity at the trailing-edge. Stewartson (refs. 24,25) points out, based on the triple-deck subset of the Navier-Stokes equations, that the skin friction has an inverse square-root singularity as the trailing-edge is approached. The displacement thickness will, however, vary smoothly through the trailing-edge region. Interacting boundary-layer theory, where upstream influence is accounted for by the boundary-condition formulation, appears to adequately calculate this flow. Melnik et al. (ref. 2) has demonstrated a similar theory for a turbulent trailing edge. To better understand the trailing-edge problem and as a test case involving strong viscous-inviscid interaction, calculations using the PNS and BL formulations described earlier are presented below.

The computation is for a flat plate, 1 m long, with $Re_L = 10^5$. The computational domain is for the interval between $x = 0.5$ and $x = 1.5$ m, with the trailing edge located at $x = 1$. Two values for the edge of

the computational domain y_e are considered. Both of these remain outside the viscous layer. The inlet conditions are Blasius, but with δ^* adjusted to account for the leading-edge interaction. The grid is unevenly spaced with 59 x-stations and 40 y-nodes, and is concentrated in the trailing-edge region where $\Delta x = 0.01$. Veldman (ref. 26) has calculated the above problem earlier with both interacting boundary-layer and triple-deck solution techniques.

Several approaches are applied to this problem. These include

1. PNS-PSD, with $y_e = 0.12$ m and $u_e = 100$ m/sec
2. BL-Direct, with surface pressures from PNS-PSD($y_e = 0.12$)
3. BL-Direct, with $\partial p/\partial x \equiv 0$ and $u_e = 100$ m/sec; this case represents noninteracting, first-order boundary-layer theory with a combined Blasius flat-plate and Goldstein near-wake solution.

Initial PNS calculations were made with the computational edge at $y_e = 0.03$, just outside the viscous region. Although the solution did exhibit upstream influence, this tendency appeared damped with unacceptable quality of agreement with the triple-deck solutions. Two possibilities were explored in efforts to explain this disagreement. One involved the incorporation of the remaining viscous terms into the algorithm(e.g., $(\mu u_x)_x$, $(\mu v_y)_y$, and $(\mu v_x)_x$). Stable spatial marching occurred for the full Navier-Stokes equations and the solutions actually presented are full Navier-Stokes solutions. However, these solutions showed only very minor changes from the PNS solutions and did not explain the disagreement above. With this extension to the full Navier-Stokes equations, the organization of the present primitive-variable formulation is similar to the streamfunction/vorticity formulation of Murphy.

The reason behind this disagreement was found, however, to lie in the second possibility. Examination of the pressure-contour plot for the PNS-PSD ($y_e = 0.03$) case (see fig. 10) revealed pressure contours that appeared to be constrained by the edge of the computational domain. To alleviate this constraint, the computational edge was moved outward in several stages to $y_e = 0.12$. The extent of upstream influence increased toward the triple-deck solution, after which no further changes occurred. Figure 11 depicts the pressure contours for the PNS-PSD ($y_e = 0.12$) case

and should be contrasted with the data in figure 10. Note the different y-scales in figures 10 and 11. We see that the distortion of the pressure field by the trailing-edge propogates nearly to the inlet boundary for the $y_e = 0.12$ case.

Except for a small range of x-stations very close to the trailing edge, much of the pressure-field adjustment occurs in the inviscid region and $\partial p/\partial y \approx 0$ within the viscous region. The relative success of interacting boundary-layer theory for the trailing-edge problem is traceable to the validity of the assumption of a zero normal pressure gradient for much of the boundary-layer and wake viscous regions. To verify this, the surface pressures from the PNS-PSD ($y_e = 0.12$) calculations were applied as the input to the BL-Direct mode. As will be seen, reasonable agreement with Veldman's results are obtained.

Figures 12 and 13 show distributions of the skin-friction coefficient C_f versus x, and the displacement thickness δ^* versus x for the three cases. Figure 14 shows the distribution of the normalized wake centerline velocity u_{CL}/u_e versus x. Also included is the triple-deck-based solution of Veldman. The PNS-PSD ($y_e = 0.12$) case shows excellent agreement with Veldman's results, confirming that the present formulation is capable of correctly accounting for both the viscous and inviscid regions of this strong viscous-inviscid interaction flow. The results for the BL-Direct (with PNS-PSD surface pressure) case prove to be quite acceptable, with differences occurring for δ^* closest to the trailing edge, where the assumption of a zero normal pressure gradient is invalid. The skin-friction agreement is excellent, probably because the correct surface pressures are being applied. For the trailing-edge flow, the most significant effect of the viscous-inviscid interaction is to force the inviscid region to adjust the pressure field as applied to the viscous region.

The source of this pressure-field readjustment is indicated in a comparison of figures 15 and 16, which depict the streamline pattern for the noninteracting BL-Direct mode ($\partial p/\partial x \equiv 0$) and the BL-Direct mode (with PNS-PSD surface pressure). The streamline patterns for the PNS-PSD calculations are quite similar to those in figure 16. For the BL-Direct ($\partial p/\partial x \equiv 0$) calculations, a discontinuity develops in the streamlines at

the trailing-edge. This streamline discontinuity is the result of the sudden acceleration of the innermost portion of the viscous layer upon release of the no-slip condition, a discontinuous change in boundary condition. Consider that the y-momentum equation can be written as $\partial p/\partial y \equiv -\rho u^2/R$; R is the radius of curvature of the local streamline. At the trailing edge, the discontinuity in streamlines implies that $R \mapsto 0$ and $\partial p/\partial y \mapsto \infty$. Thus, the streamline pattern generated by the BL-Direct ($\partial p/\partial x \equiv 0$) calculation is in sharp contradiction with the first-order boundary-layer theory assumption that $\partial p/\partial y \equiv 0$. If the y-momentum equation is incorporated or the edge-pressure boundary condition is allowed to adjust to account for upstream influence, then the pressure field will adapt to smooth out the streamline curvature until a consistent solution is obtained.

CONCLUDING REMARKS

Progress on the development of a parabolized Navier-Stokes solution method suitable for application to strong viscous-inviscid interactions has been described. An improved algorithm and boundary-condition treatment, which enhances rapid convergence to accurate solutions on coarse grids while retaining stable marching for small marching steps, is reported. To provide for proper upstream influence, the algorithmic formulation performs iterative sweeps in the x-direction and requires global storage only for pressure. The method has been validated through the successful computation of two subsonic, strong viscous-inviscid interactions, including a separation bubble and a trailing edge. Detailed comparison with Navier-Stokes solutions and triple-deck theory is made with excellent agreement indicated.

The improved algorithm stems from a conceptual reinterpretation of stability requirements presented earlier by Rubin. In the present work, this stability requirement for forward-differencing of $\partial p/\partial x$ is removed. Rather, this paper demonstrates that stable, subsonic marching of the PNS equations merely requires that the pressure variable being solved for should be the trailing pressure in the $\partial p/\partial x$ term. This idea is used to formulate the present algorithm; within each equation, consistent differencing is imple-

mented for all streamwise derivatives.

Boundary condition modes for external flows are direct pressure, inverse edge-streamfunction, and psuedodirect modes. With these boundary conditions, the present code is well suited for coupling with an inviscid code. For internal flows, global mass conservation is used. The boundary-condition treatment proves crucial in enhancing rapid convergence. For these strong viscous-inviscid interactions, the global constraints imposed by the inverse and psuedodirect boundary conditions provide the improvement in robustness over the direct boundary condition required to make this formulation a practical and useful approach.

The computations for strong viscous-inviscid interactions demonstrates that the present PNS algorithm and boundary-condition formulation is a rapid, accurate, and robust approach which incorporates the essential features of elliptic upstream influence. For the trailing-edge flow, the PNS algorithm was extended to include the full Navier-Stokes terms with stable spatial marching achieved. To this author's knowledge, this is the first successful spatially marched calculations of the full Navier-Stokes equations in primitive variable form for subsonic, strong viscous-inviscid interactions.

The inclusion of a zero- and a two-equation turbulence model, and the incorporation of the compressible terms into the present code, recommendations for future work, have already been partially implemented. The combination of a turbulent compressible version of the present PNS code with an Euler solver in a coupling procedure should then be accomplished. The code would then serve as an efficient computational tool in turbulence modeling studies of strong viscous-inviscid interactions.

APPENDIX: MATRIX ELEMENTS

The matrix system being solved is of the form

$$(A_{k,m})_j(U_m)_{j-1} + (B_{k,m})_j(U_m)_j + (C_{k,m})_j(U_m)_{j+1} = (D_k)_j \qquad (A1)$$

where

j =1, $jmax$ refers to the jth differencing molecule

k refers to the equation:

=1, continuity

=2, x-momentum

=3, y-momentum

m refers to the variable:

=1, $(U_1)_j \equiv \Delta v_{i,j} = v_{i,j} - v_{i-1,j}$

=2, $(U_2)_j \equiv \Delta u_{i,j} = u_{i,j} - u_{i-1,j}$

=3, $(U_3)_j \equiv p_{i-1,j}$

The interior elements for the continuity equation are

$$\begin{aligned}
\Delta v_{j-1}: &\quad (A_{11})_j = -1 \\
\Delta u_{j-1}: &\quad (A_{12})_j = 0.5 \cdot BX0 \cdot DYX - DEXM \\
p_{i-1,j-1}: &\quad (A_{13})_j = 0 \\
\\
\Delta v_j: &\quad (B_{11})_j = 1 \\
\Delta u_j: &\quad (B_{12})_j = 0.5 \cdot BX0 \cdot DYX + DEXM \\
p_{i-1,j}: &\quad (B_{13})_j = 0 \\
\\
\Delta v_{j+1}: &\quad (C_{11})_j = 0 \\
\Delta u_{j+1}: &\quad (C_{12})_j = 0 \\
p_{i-1,j+1}: &\quad (C_{13})_j = 0 \\
&\quad (D_1)_j = -(v^n_{i-1,j} - v^n_{i-1,j-1}) \\
&\qquad - (u^n_{i-1,j} - u^n_{i-1,j-1}) \cdot DEXM \\
&\qquad + 0.5 \cdot DYX \cdot BX2 \cdot [(u^n_{i-1,j} + u^n_{i-1,j-1}) \\
&\qquad\qquad - (u^n_{i-2,j} + u^n_{i-2,j-1})]
\end{aligned} \qquad (A2)$$

The interior elements for the x-momentum equation are

$$
\begin{aligned}
\Delta v_{j-1}: \quad & (A_{21})_j = 0 \\
\Delta u_{j-1}: \quad & (A_{22})_j = RX \cdot CYM - DTM \\
p_{i-1,j-1}: \quad & (A_{23})_j = 0 \\
\\
\Delta v_j: \quad & (B_{21})_j = 0 \\
\Delta u_j: \quad & (B_{22})_j = (\rho u)^n_{i,j} \cdot BX0 + RX \cdot CY0 \\
& \qquad + (DTP + DTM) \\
p_{i-1,j}: \quad & (B_{23})_j = BX1 \\
\\
\Delta v_{j+1}: \quad & (C_{21})_j = 0 \\
\Delta u_{j+1}: \quad & (C_{22})_j = RX \cdot CYP - DTP \\
p_{i-1,j+1}: \quad & (C_{23})_j = 0
\end{aligned}
\tag{A3}
$$

$$
\begin{aligned}
(D_2)_j = & -(\rho u)^n_{i,j} \cdot BX2 \cdot (u^n_{i-2,j} - u^n_{i-1,j}) \\
& - RX \cdot (CYP \cdot u^n_{i-1,j+1} + CY0 \cdot u^n_{i-1,j} \\
& \qquad + CYM \cdot u^n_{i-1,j-1}) \\
& + DTP \cdot (u^n_{i-1,j+1} - u^n_{i-1,j}) \\
& + DTM \cdot (u^n_{i-1,j-1} - u^n_{i-1,j}) \\
& - DEX \cdot (CYP \cdot p^{n-1}_{i,j+1} + CY0 \cdot p^{n-1}_{i,j} \\
& \qquad + CYM \cdot p^{n-1}_{i,j-1}) \\
& - (BX0 \cdot p^{n-1}_{i,j} + BX2 \cdot p^n_{i-2,j})
\end{aligned}
$$

Note that the $(\rho u)^n_{i,j}$ and RX terms are found through iteration.

The interior elements for the y-momentum equation are

$$
\begin{aligned}
\Delta v_{j-1}: &\quad (A_{31})_j = 0 \\
\Delta u_{j-1}: &\quad (A_{32})_j = 0 \\
p_{i-1,j-1}: &\quad (A_{33})_j = 0
\end{aligned}
$$

$$
\begin{aligned}
\Delta v_j: &\quad (B_{31})_j = -0.5 \cdot DYM \cdot CXP \cdot (\rho u)^n_{i-1,j} \\
\Delta u_j: &\quad (B_{32})_j = 0.5 \cdot DYM \cdot CXP \cdot (\rho v)^n_{i-1,j} \\
p_{i-1,j}: &\quad (B_{33})_j = -1
\end{aligned}
$$

$$
\begin{aligned}
\Delta v_{j+1}: &\quad (C_{31})_j = -0.5 \cdot DYM \cdot CXP \cdot (\rho u)^n_{i-1,j+1} \\
\Delta u_{j+1}: &\quad (C_{32})_j = 0.5 \cdot DYM \cdot CXP \cdot (\rho v)^n_{i-1,j+1} \\
p_{i-1,j+1}: &\quad (C_{33})_j = 1
\end{aligned}
$$

$$
\begin{aligned}
(D_2)_j = &-0.5 \cdot DYM \cdot CXM \cdot [(\rho v)^n_{i-1,j}(u^n_{i-2,j} - u^n_{i-1,j}) \\
&\qquad + (\rho v)^n_{i-1,j+1}(u^n_{i-2,j+1} - u^n_{i-1,j+1})] \\
&+ 0.5 \cdot DYM \cdot CXM \cdot [(\rho u)^n_{i-1,j}(v^n_{i-2,j} - v^n_{i-1,j}) \\
&\qquad + (\rho u)^n_{i-1,j+1}(v^n_{i-2,j+1} - v^n_{i-1,j+1})] \\
&+ 0.5 \cdot DEXP \cdot [(\rho v)^n_{i-1,j} + (\rho v)^n_{i-1,j+1}] \\
&\qquad \cdot (u^n_{i-1,j+1} - u^n_{i-1,j}) \\
&- 0.5 \cdot DEXP \cdot [(\rho u)^n_{i-1,j} + (\rho u)^n_{i-1,j+1}] \\
&\qquad \cdot (v^n_{i-1,j+1} - v^n_{i-1,j})
\end{aligned}
\tag{A4}
$$

where

$$
\begin{aligned}
DX &= x_i - x_{i\text{-}1} \\
DX2R &= (x_i - x_{i\text{-}1})/(x_i - x_{i\text{-}2}) \\
BX1 &= -(x_i - x_{i\text{-}2})/(x_{i\text{-}1} - x_{i\text{-}2}) \\
BX0 &= -BX1/(1 - DX2R \cdot DX2R) \\
BX2 &= -(BX0 + BX1) \\
CXP &= \quad (x_{i\text{-}1} - x_{i\text{-}2})/[(x_i - x_{i\text{-}2})(x_i - x_{i\text{-}1})] \\
CXM &= -(x_i - x_{i\text{-}1})/[(x_i - x_{i\text{-}2})(x_{i\text{-}1} - x_{i\text{-}2})] \\
CX0 &= -(CXP + CXM) \\
CYP &= \quad (y_{i,j} - y_{i,j\text{-}1})/[(y_{i,j+1} - y_{i,j})(y_{i,j+1} - y_{i,j\text{-}1})] \\
CYM &= \quad (y_{i,j+1} - y_{i,j})/[(y_{i,j} - y_{i,j\text{-}1})(y_{i,j+1} - y_{i,j\text{-}1})] \\
CY0 &= -(CYP + CYM) \\
DYX &= (y_{i,j} - y_{i,j\text{-}1})/(x_i - x_{i\text{-}1}) \\
DYM &= (y_{i\text{-}1,j+1} - y_{i\text{-}1,j}) \\
DEX &= -(y_{i,j} - y_{i\text{-}1,j}) \\
DEXM &= -0.5 \cdot [(y_{i,j} - y_{i,j\text{-}1}) \\
&\qquad - (y_{i\text{-}1,j} - y_{i\text{-}1,j\text{-}1})]/(x_i - x_{i\text{-}1}) \\
DEXP &= -0.5 \cdot [(y_{i,j} - y_{i,j+1}) \\
&\qquad - (y_{i\text{-}2,j} - y_{i\text{-}2,j\text{-}1})]/(x_i - x_{i\text{-}2}) \\
DTP &= DX \cdot (\mu_{i,j+1} + \mu_{i,j}) \\
&\qquad /[(y_{i,j+1} - y_{i,j\text{-}1}) \cdot (y_{i,j+1} - y_{i,j})] \\
DTM &= DX \cdot (\mu_{i,j} + \mu_{i,j\text{-}1}) \\
&\qquad /[(y_{i,j+1} - y_{i,j\text{-}1}) \cdot (y_{i,j} - y_{i,j\text{-}1})] \\
RX &= (\rho v)^n_{i,j} \cdot DX + (\rho u)^n_{i,j} \cdot DEX
\end{aligned}
$$

REFERENCES

1. Van Dyke, M.: Higher-Order Boundary-Layer Theory. **Annual Review of Fluid Mechanics**, vol. 1, Annual Reviews, Inc., Palo Alto, Calif., 1969, pp. 265-292.

2. Melnik, R. E.; Chow, R.; and Mead, H. R.: Theory of Viscous Transonic Flow over Airfoils at High Reynolds Number. AIAA Paper 77-680, 1977.

3. Lock, R. C.: A Review of Methods for Predicting Viscous Effects on Aerofoils and Wings at Transonic Speeds. AGARD Symposium on Computation of Viscous-Inviscid Interactions, AGARD CP-291, 1980.

4. Le Balleur, J. C.; Peyret, R.; and Viviand, H.: Numerical Studies in High Reynolds Number Aerodynamics. **Computers and Fluids**. vol. 8, 1980, pp. 1-30.

5. Beam, R. M.; and Warming, R. F.: An Implicit Factored Scheme for the Compressible Navier-Stokes Equations. **AIAA J.**, vol. 16, no. 4, Apr. 1978, pp. 393-402.

6. Vigneron, Y. C.; Rakich, J. V.; and Tannehill, J. C.: Calculation of Supersonic Viscous Flow over Delta Wings with Sharp Subsonic Leading Edges. AIAA Paper 78-1137, 1978.

7. Schiff, L. B.; and Steger, J. L.: Numerical Simulation of Steady Supersonic Viscous Flow. AIAA Paper 79-0130, 1979.

8. Patankar, S. V.: **Numerical Heat Transfer and Fluid Flow**. Hemisphere Publishing Corporation. New York, 1980.

9. Madavan, N. K.; and Pletcher, R. H.: Prediction of Incompressible Laminar Separated Flows Using the Partially Parabolized Navier-Stokes Equations. Technical Report HTL-27, ISU-ERI-Ames-82127, Engineering Research Institute, Iowa State U., 1982.

10. Rubin, S. G.: A Review of Marching Procedures for Parabolized Navier-Stokes Equations. Proceedings of a Symposium on Numerical and Physical Aspects of Aerodynamic Flows, Springer-Verlag, 1982, pp. 171-186.

11. Lin, A.; and Rubin, S. G.: Three-Dimensional Supersonic Viscous Flow over a Cone at Incidence. **AIAA J.**, vol. 20, no. 11, Nov. 1982, pp. 1500-1507.

12. Maghoub, H. E. H.; and Bradshaw, P.: Calculation of Turbulent-Inviscid Interactions with Large Normal Pressure Gradients. **AIAA J.**, vol. 17, no. 10, Oct. 1979, pp. 1025-1029.

13. Chen, Z. B.; and Bradshaw, P.: Calculations of Viscous Transonic Flow over Aerofoils. AIAA Paper 82-0997, 1982.

14. Rubin, S. G.; and Reddy, D. R.: Global Solution Procedures for Incompressible Laminar Flow with Strong Pressure Interaction and Separation. Presented at 2nd Symposium on Numerical and Physical Aspects of Aerodynamic Flows, Jan. 1983.

15. Reyhner, T. A.; and Flügge-Lotz, I.: The Interaction of a Shock Wave with a Laminar Boundary Layer. **International Journal of Non-Linear Mechanics**, vol. 3, no. 2, June 1968, pp. 173-199.

16. Steger, J. L.: Implicit Finite-Difference Simulation of Flow about Arbitrary Two-Dimensional Geometries. **AIAA J.**, vol. 16, no. 7, July 1978, pp. 679-686.

17. Carter, J. E.: A New Boundary Layer Interaction Technique for Separated Flows. AIAA Paper 79-1450, 1979.

18. Briley, W. R.: A Numerical Study of Laminar Separation Bubbles Using the Navier-Stokes Equations. **J. Fluid Mech.**, vol. 47, 1971, pp. 713-736.

19. Lighthill, M. J.: On Boundary Layers and Upstream Influence. II. Supersonic Flows without Separation. **Proc. R. Soc. London**, Ser. A, vol. 217, 1953, pp. 478-507.

20. Murphy, J. D.: An Efficient Solution Procedure for the Incompressible Navier-Stokes Equations. **AIAA J.**, vol. 15, no. 9, 1977, pp. 1307-1314.

21. Pletcher, R. H.: Prediction of Incompressible Turbulent Separating Flow. **ASME J. Fluids Engineering**, vol. 100, Dec. 1978, pp. 427-433.

22. Landau, L. D.; and Lifshitz, E. M.: **Fluid Mechanics.** Pergammon Press, New York, 1975.

23. Goldstein, S.: Concerning Some Solutions of the Boundary Layer Equations in Hydrodynamics. **Proc. Cambridge Philos. Soc.**, vol. 26, 1930, pp. 1-30.

24. Stewartson, K.: On the Flow near the Trailing Edge of a Flat Plate. **Proc. R. Soc. London**, Ser. A, vol. 306, 1969, pp. 275-290.

25. Stewartson, K.: Multistructured Boundary Layers on Flat Plates and Related Bodies. **Adv. Appl. Mech.**, vol. 14, pp. 145-239, Academic Press, Inc., 1974.

26. Veldman, A. E. P.: Boundary Layers with Strong Interaction: From Asymptotic Theory to Calculation Method. Proceedings BAIL I Conference, Dublin, 1980, pp. 149-163.

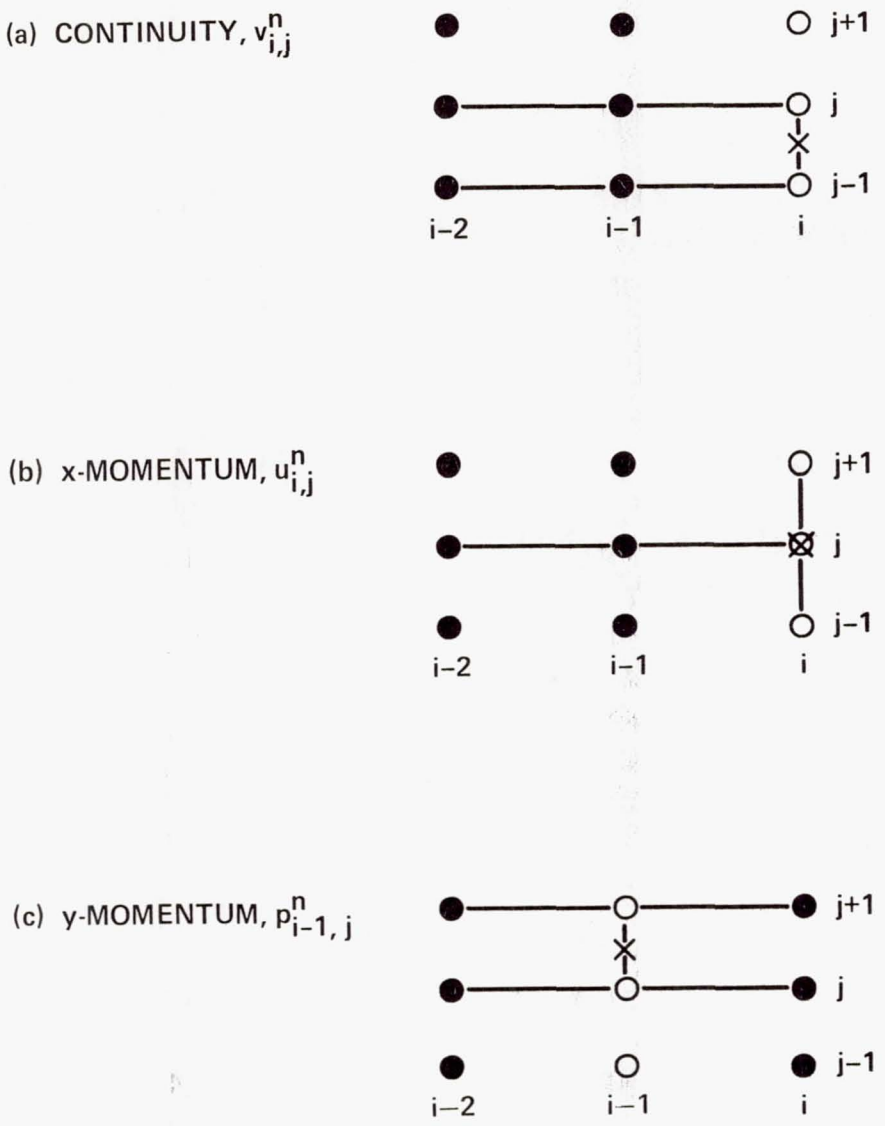

Figure 1. – Computational molecule.

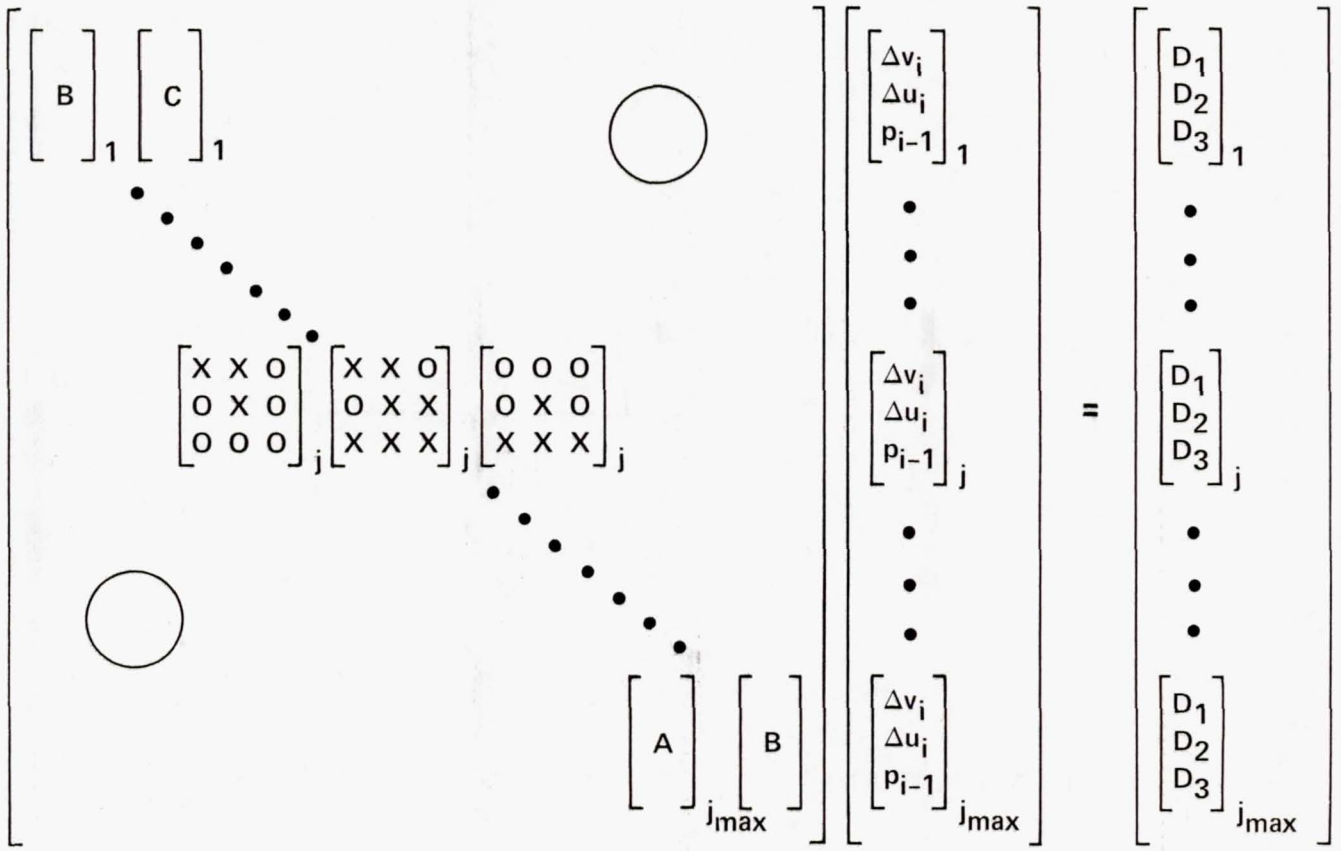

Figure 2. – Matrix structure.

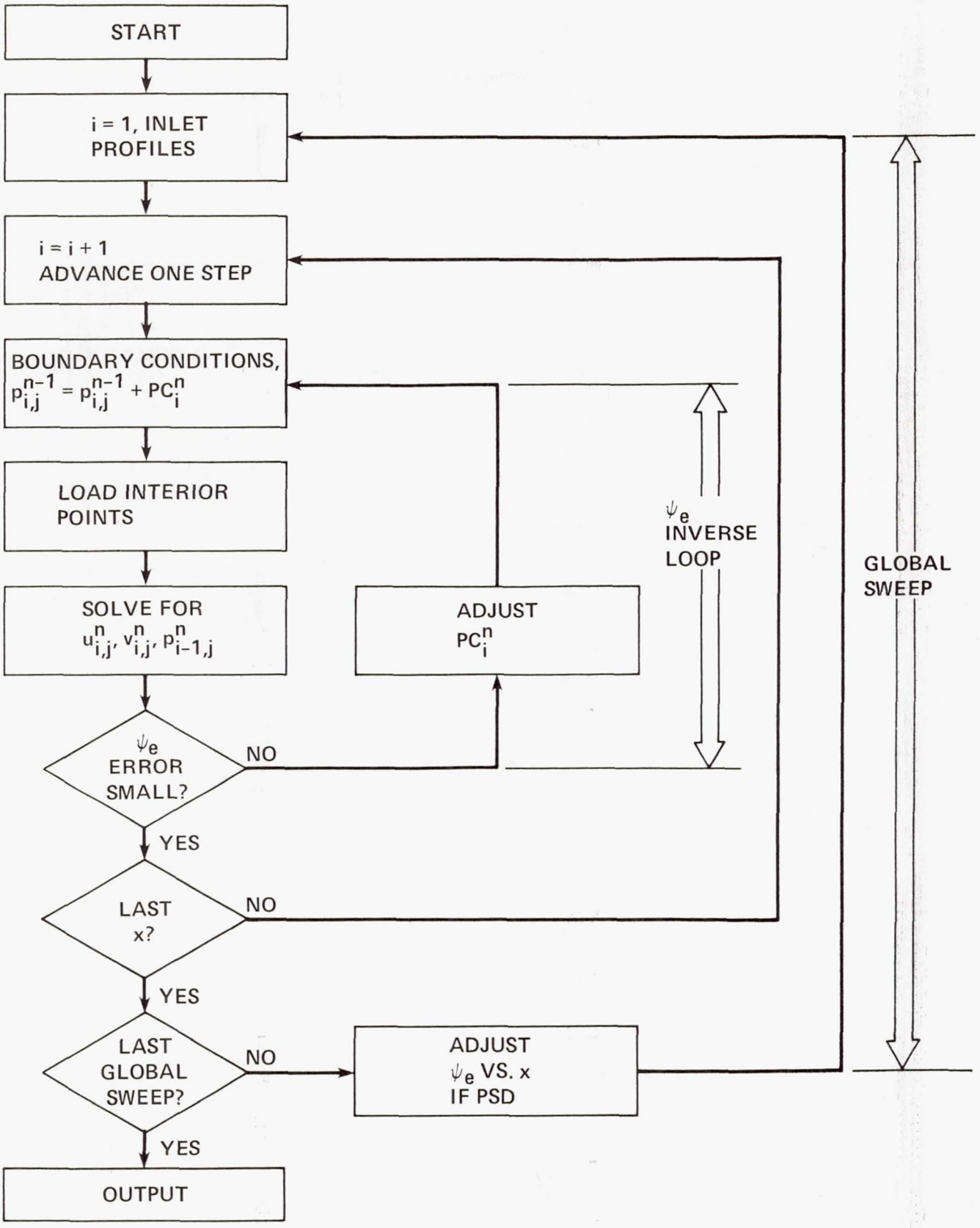

Figure 3. – Block logic for PNS-PSD mode.

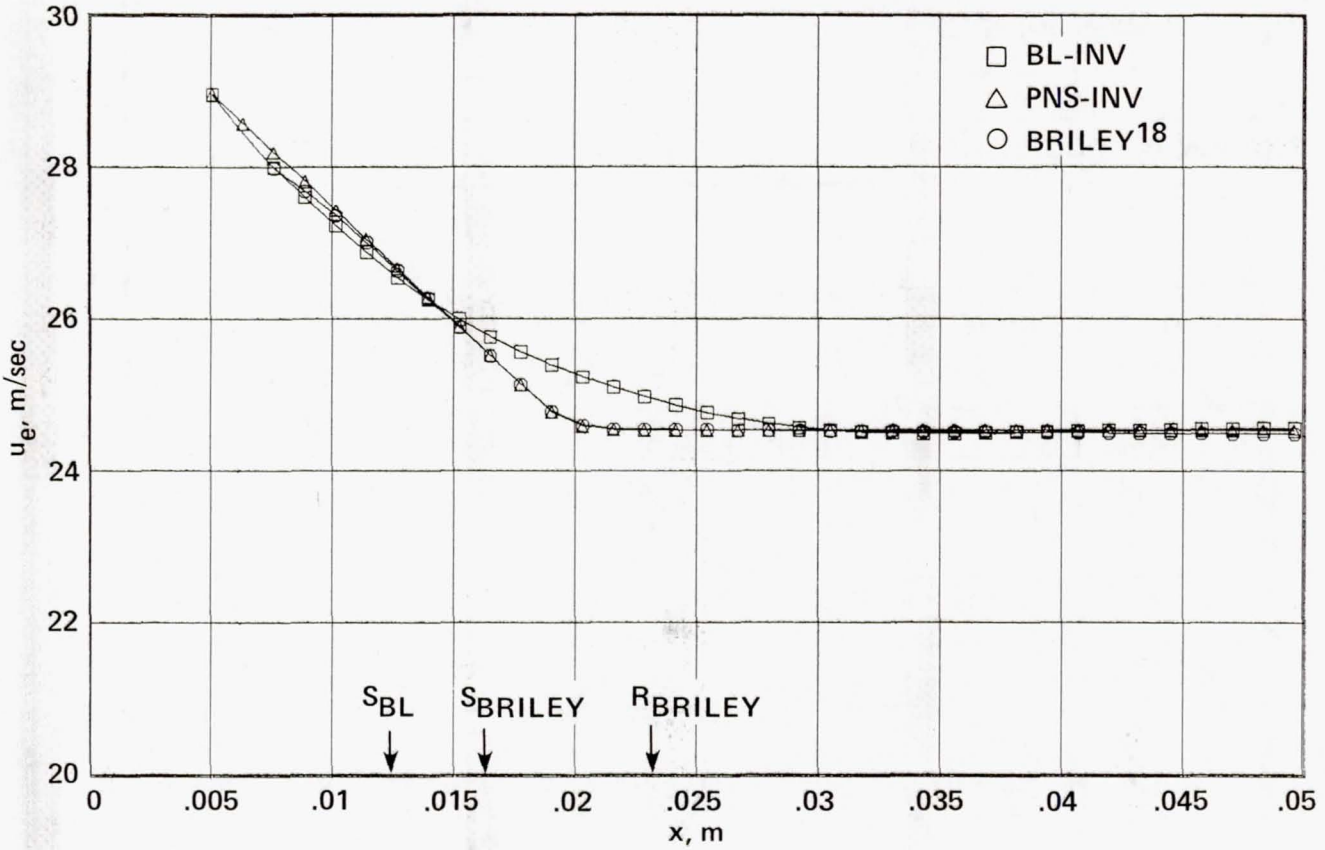

Figure 4. – Edge-velocity distribution for Briley-3 case.

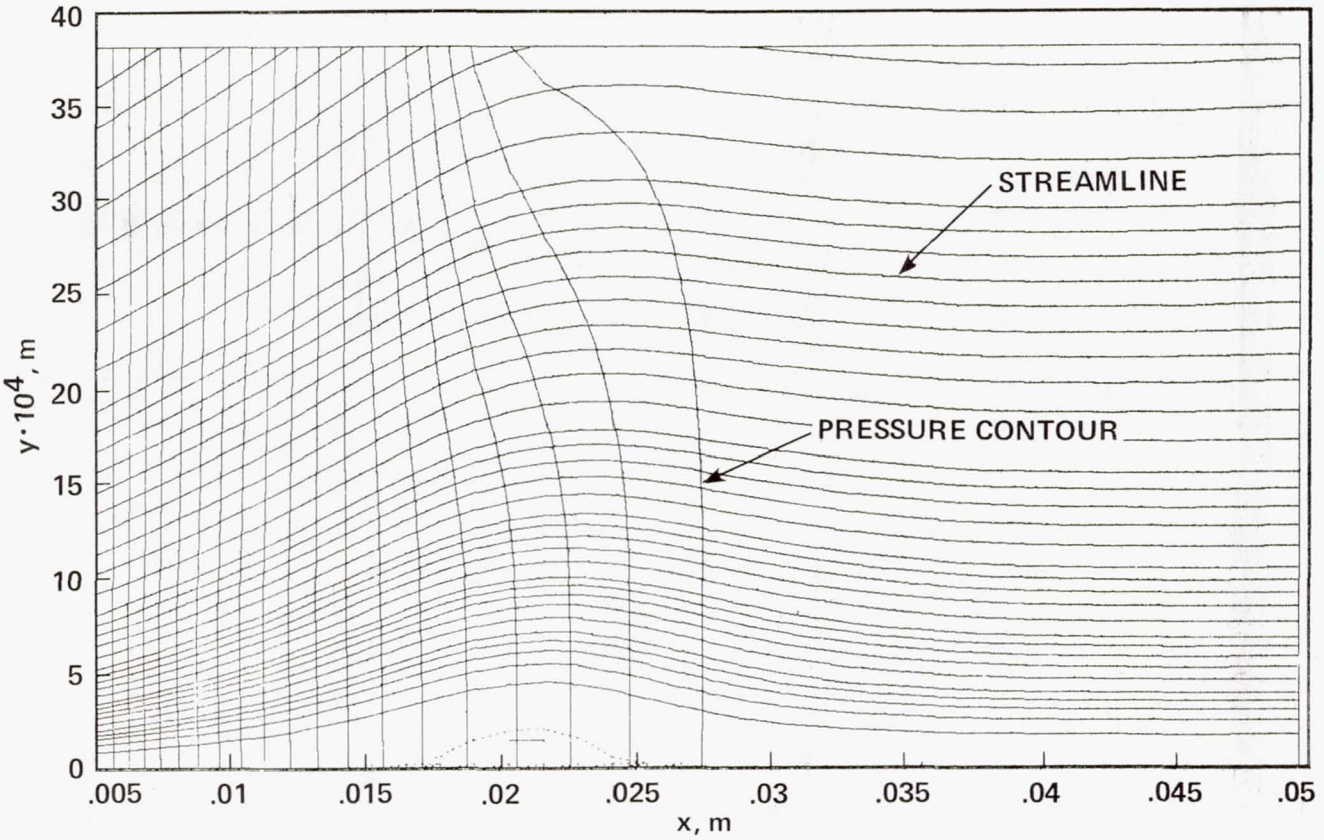

Figure 5. – Streamline and pressure contours for Briley-3 case: PNS-INV solution.

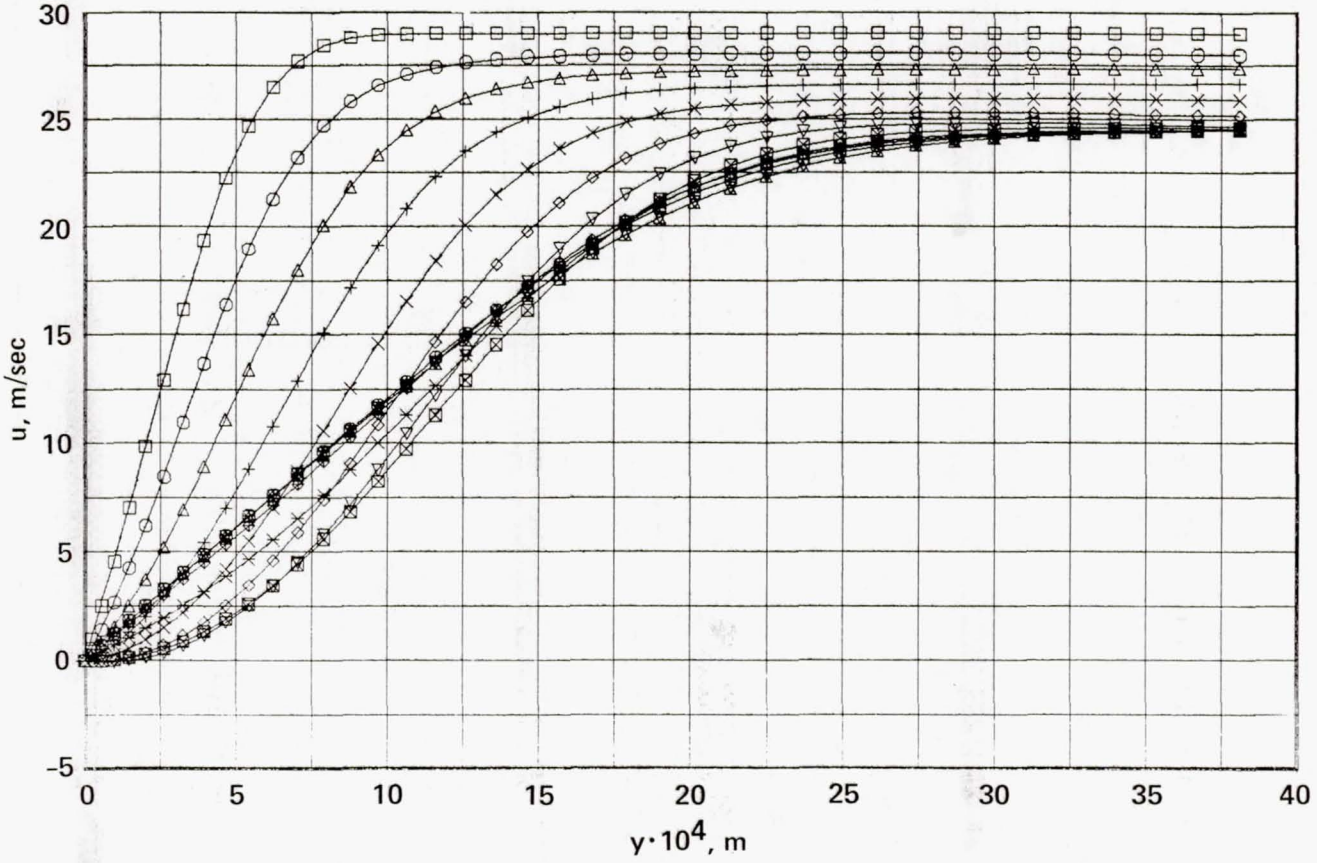

Figure 6. – Velocity profiles for Briley-3 case: PNS-INV solution.

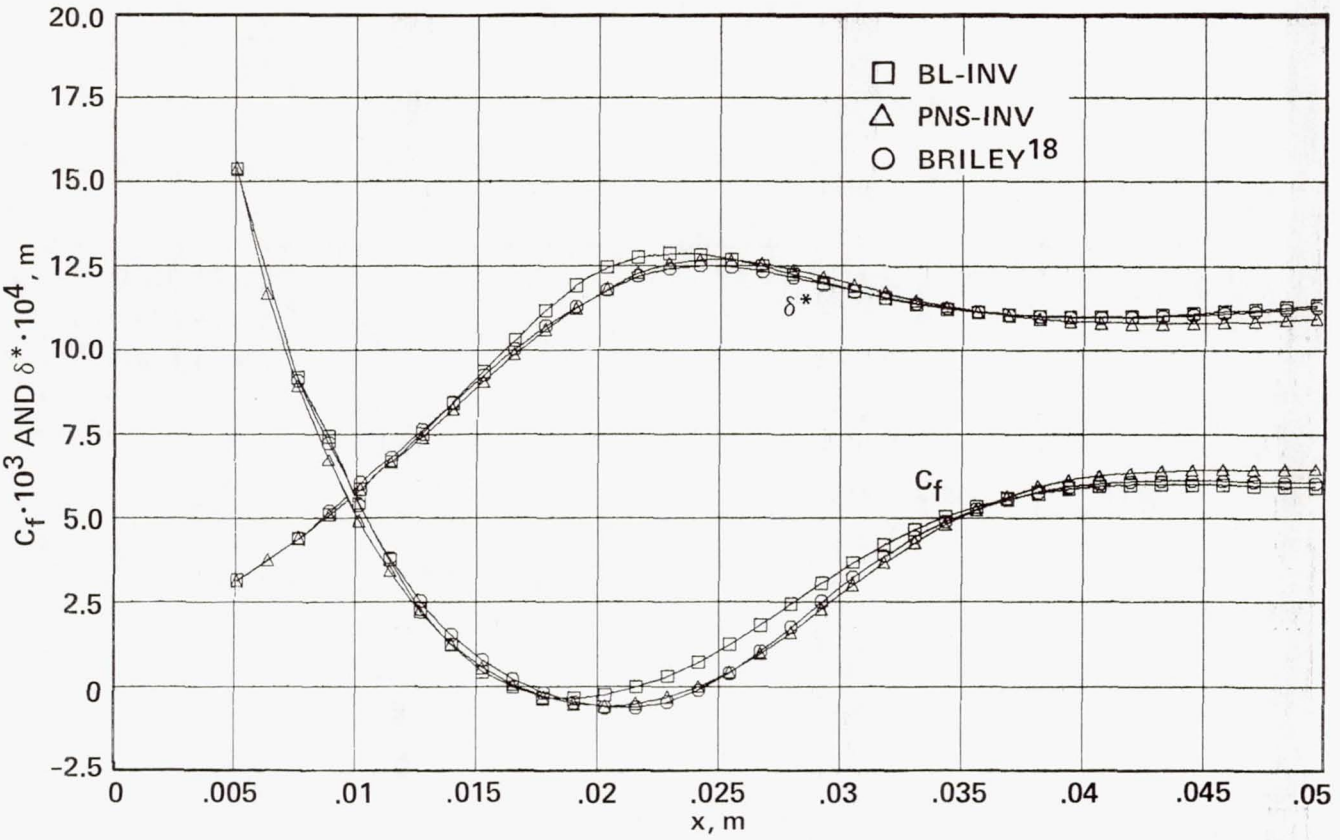

Figure 7. – Skin-friction and displacement-thickness distributions for Briley-3 case.

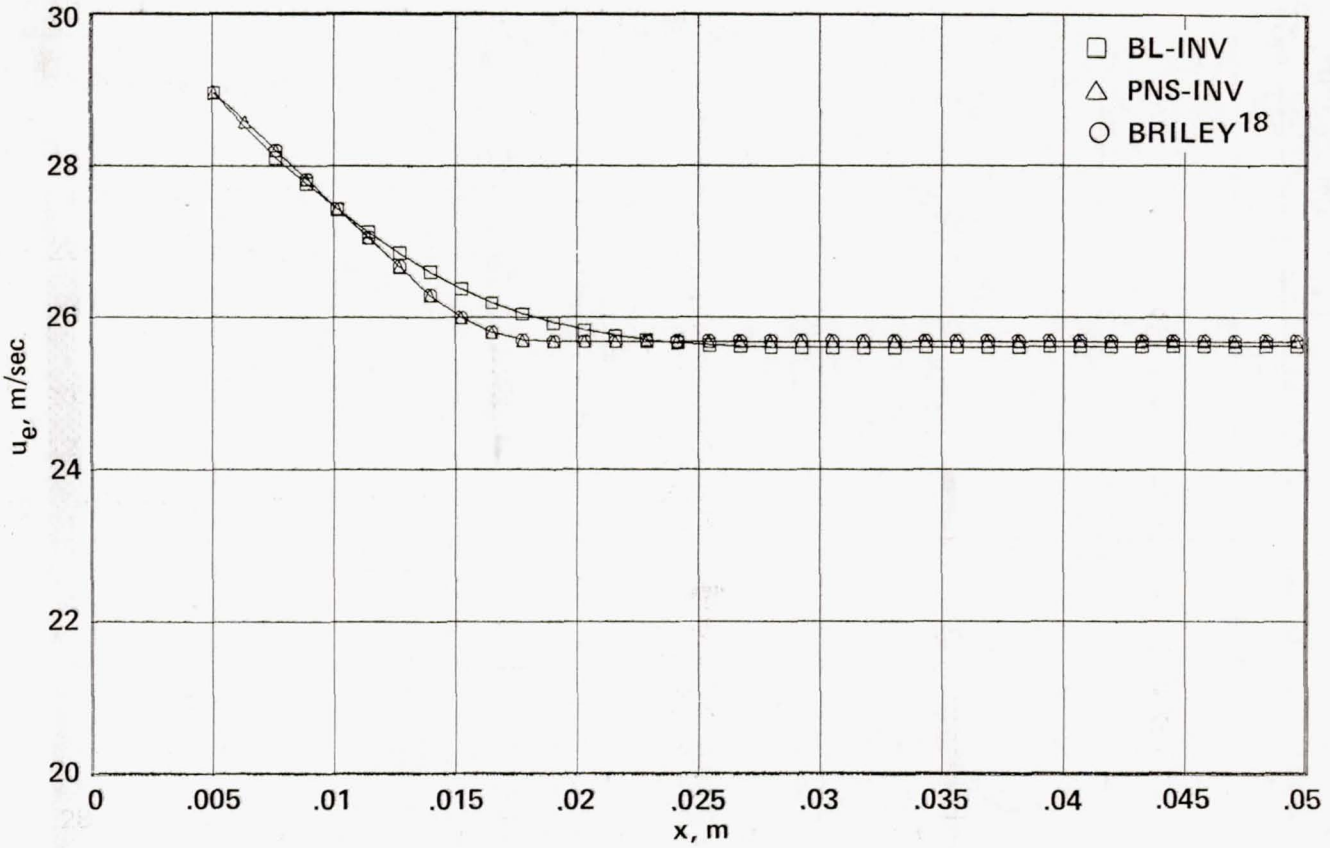

Figure 8. – Edge-velocity distribution for Briley-1 case.

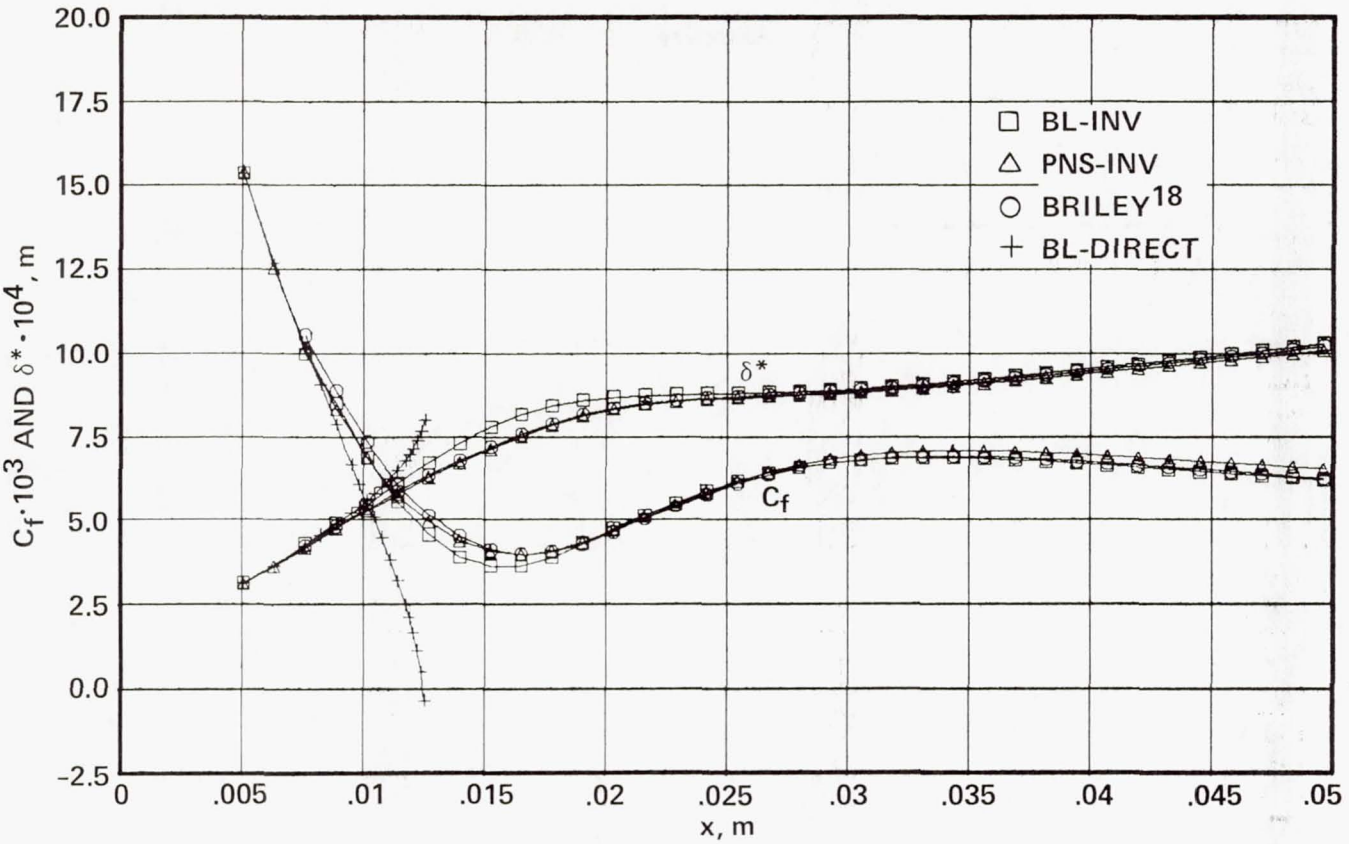

Figure 9. – Skin-friction and displacement-thickness distributions for Briley-1 case.

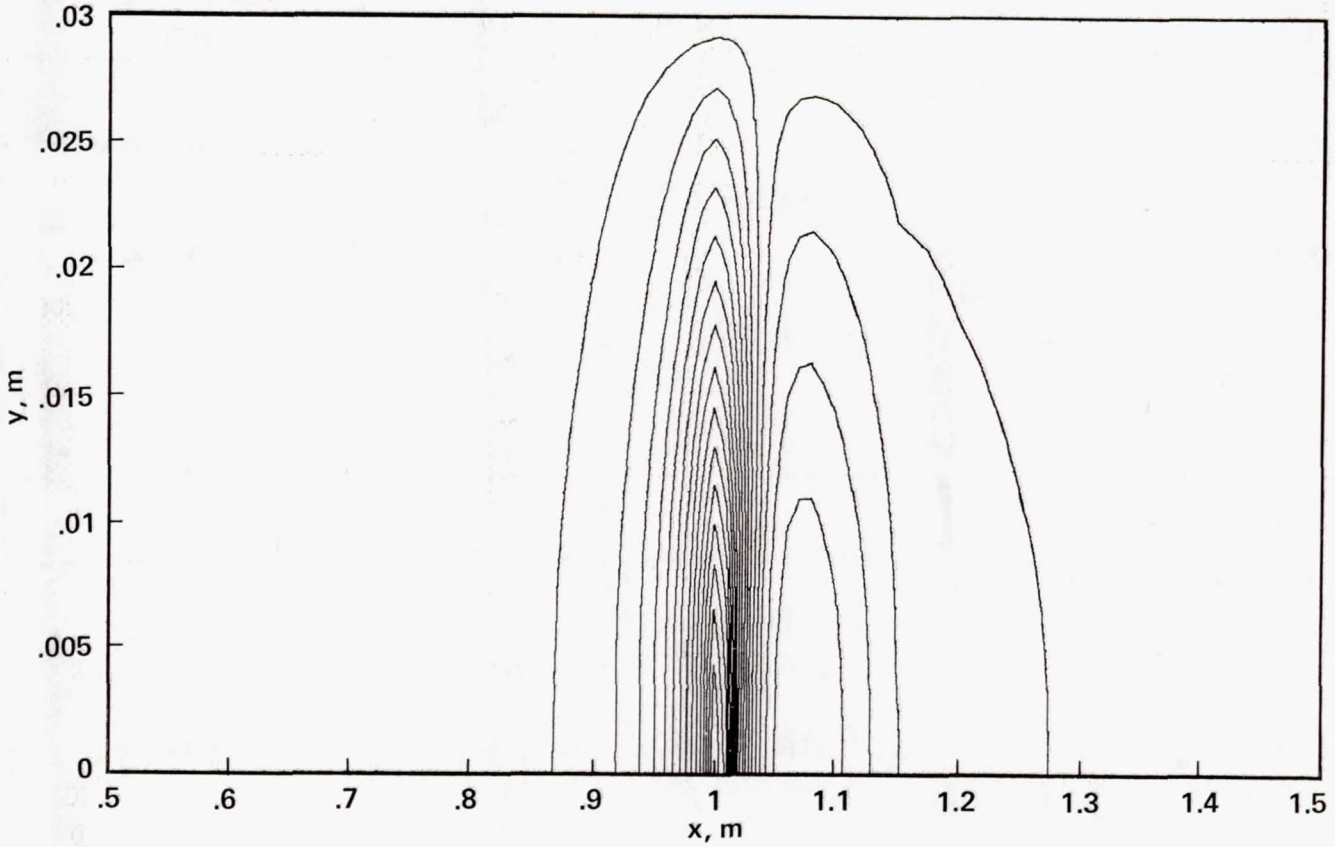

Figure 10. – Pressure contours for trailing-edge interaction: PNS-PSD with $y_e = 0.03$ m.

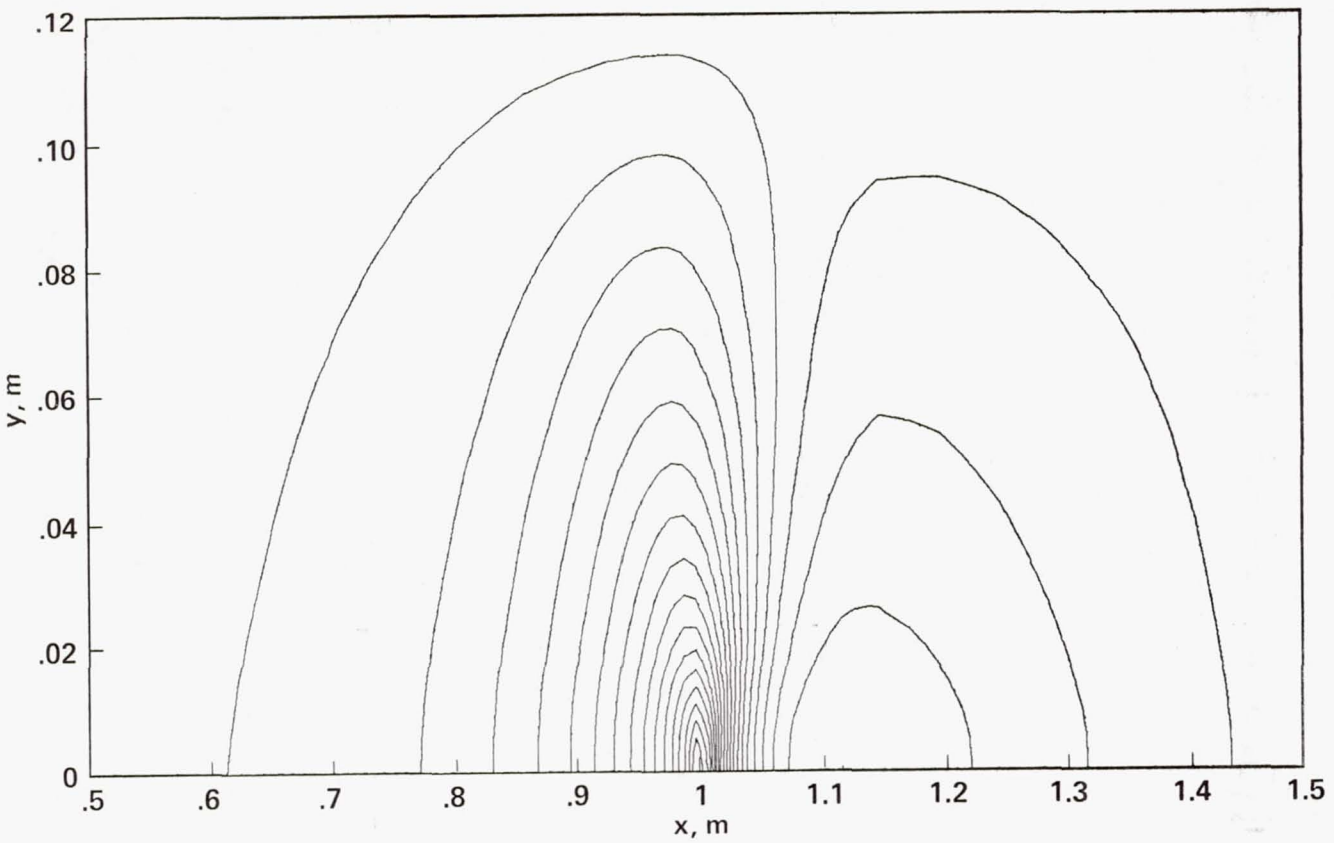

Figure 11. – Pressure contours for trailing-edge interaction: PNS-PSD with $y_e = 0.12$ m.

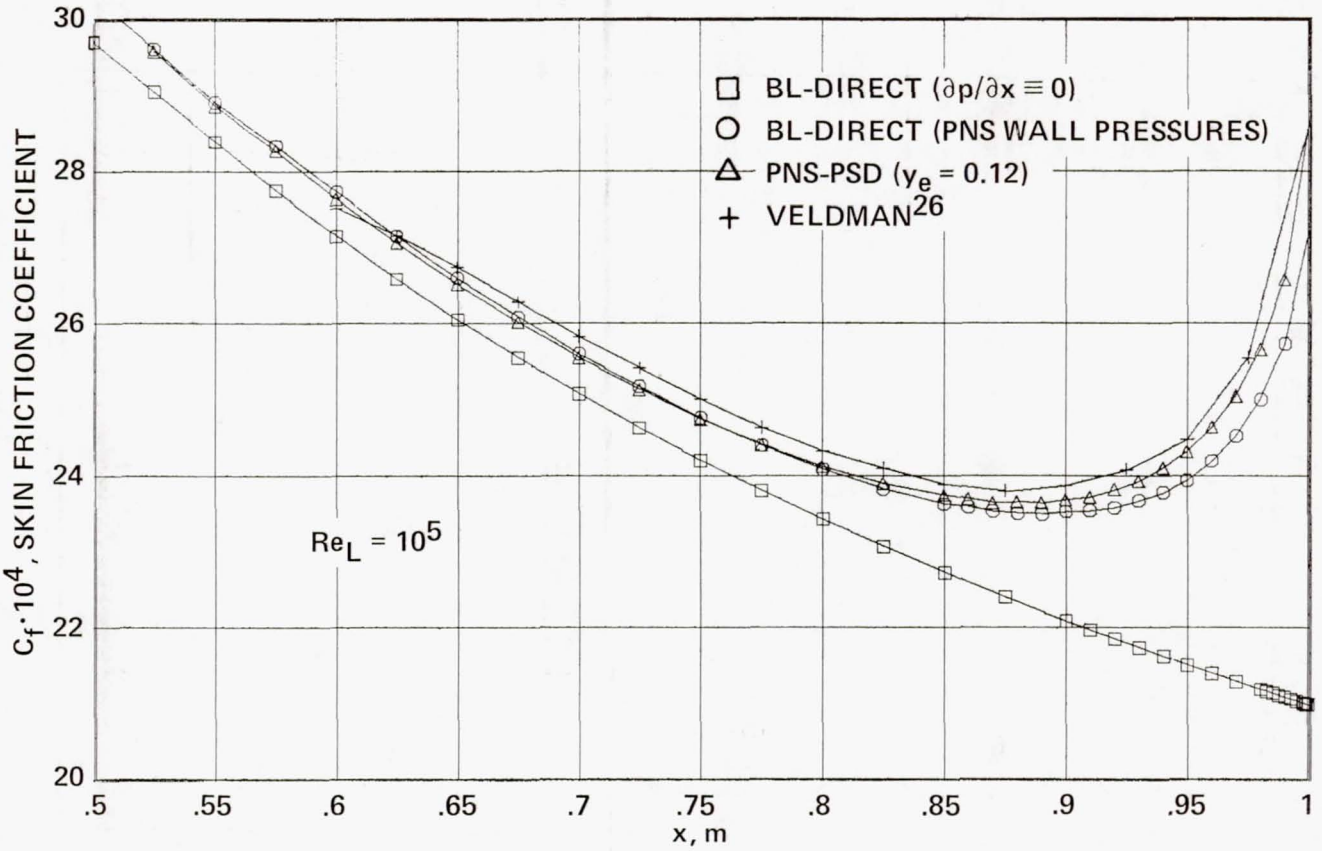

Figure 12. – Skin-friction coefficient distributions for trailing-edge interaction.

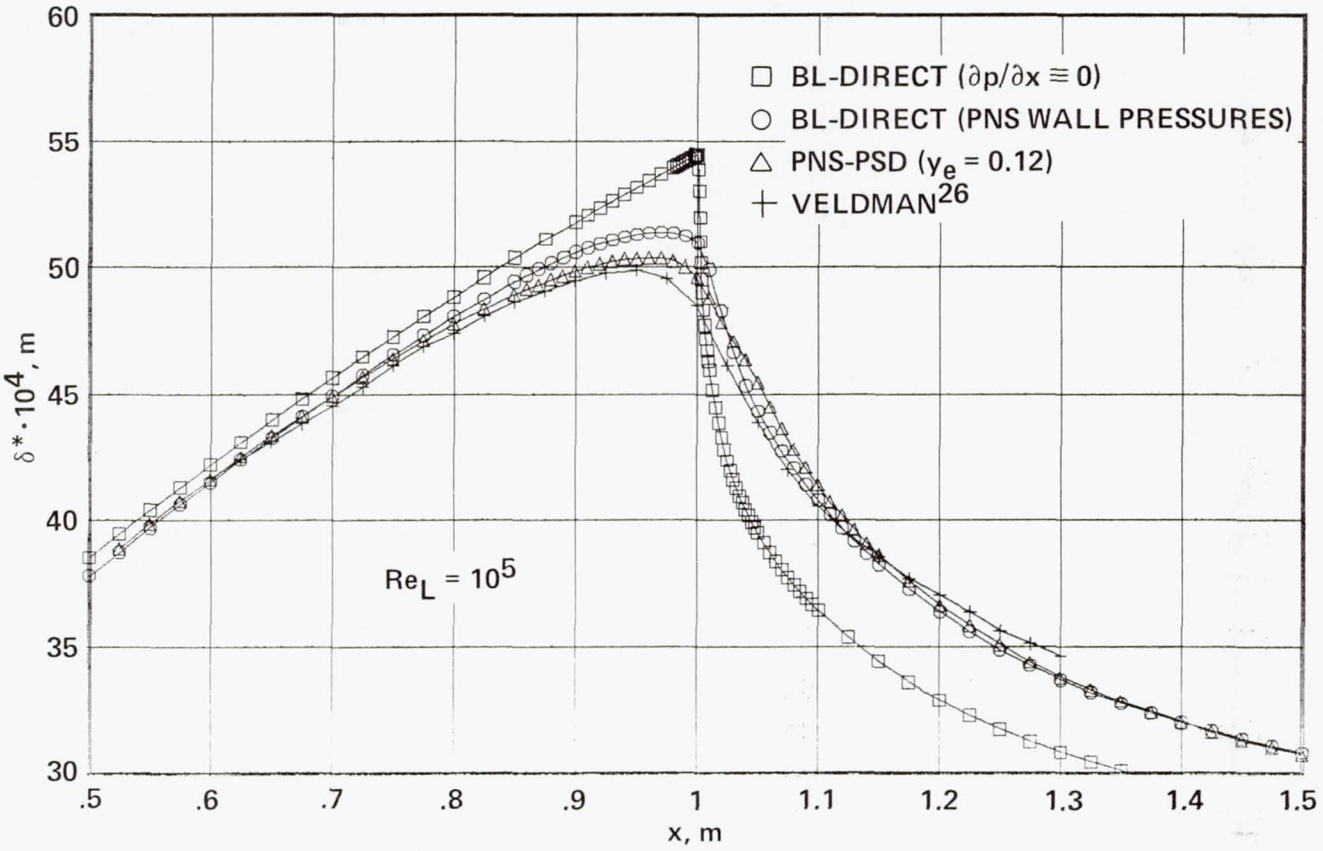

Figure 13. – Displacement-thickness distributions for trailing-edge interaction.

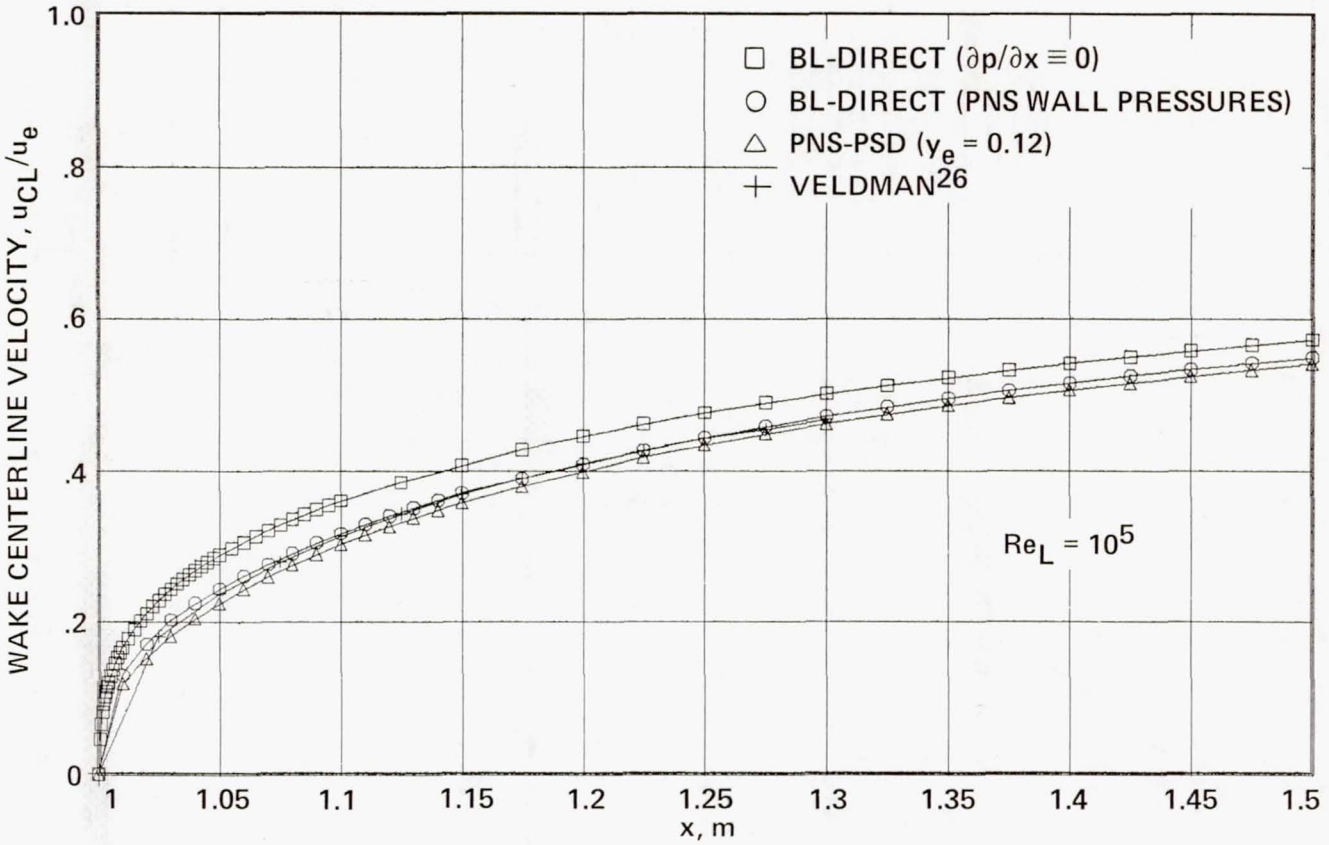

Figure 14. – Wake centerline velocity distributions for trailing-edge interaction.

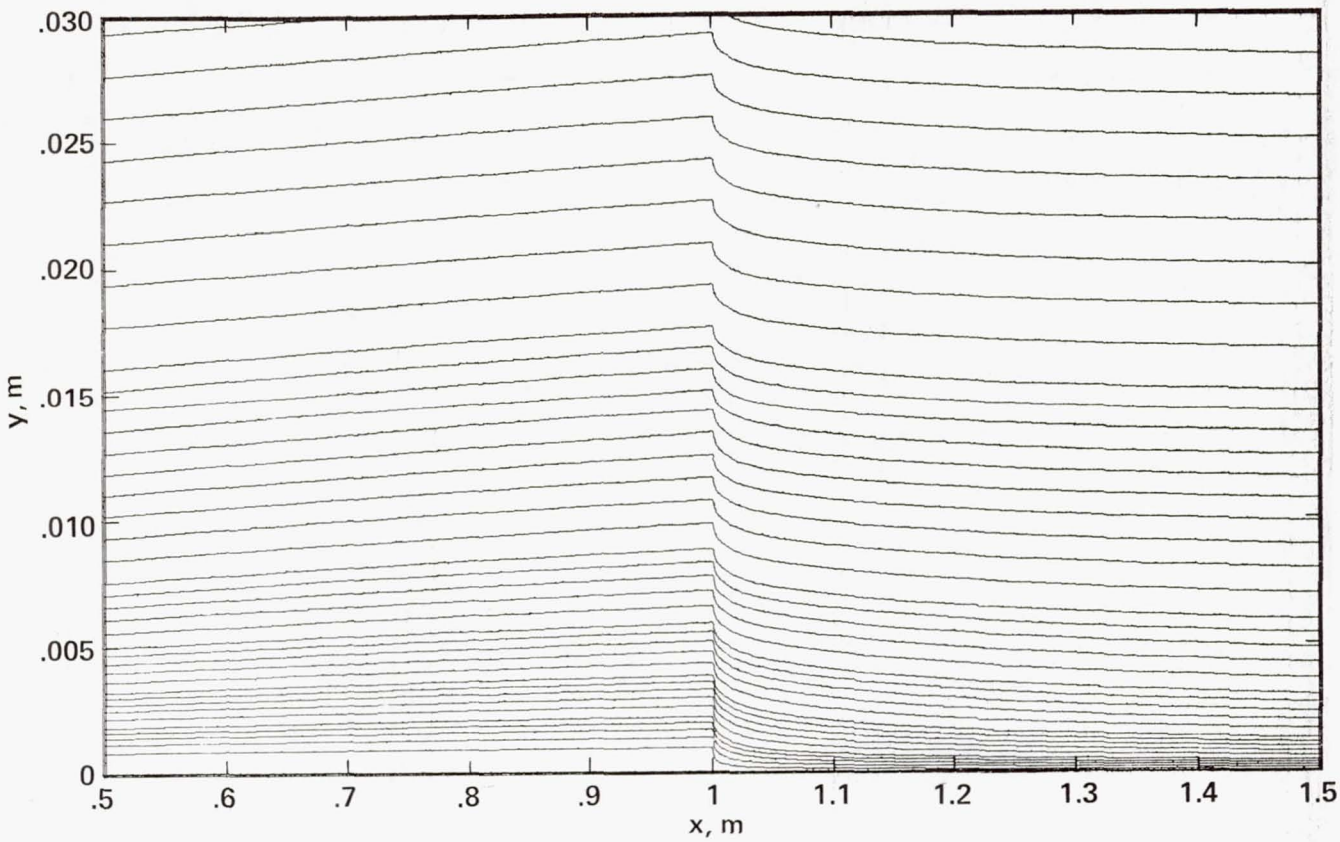

Figure 15. – Streamline contours for trailing-edge interaction: BL-Direct with $\partial p/\partial x \equiv 0$.

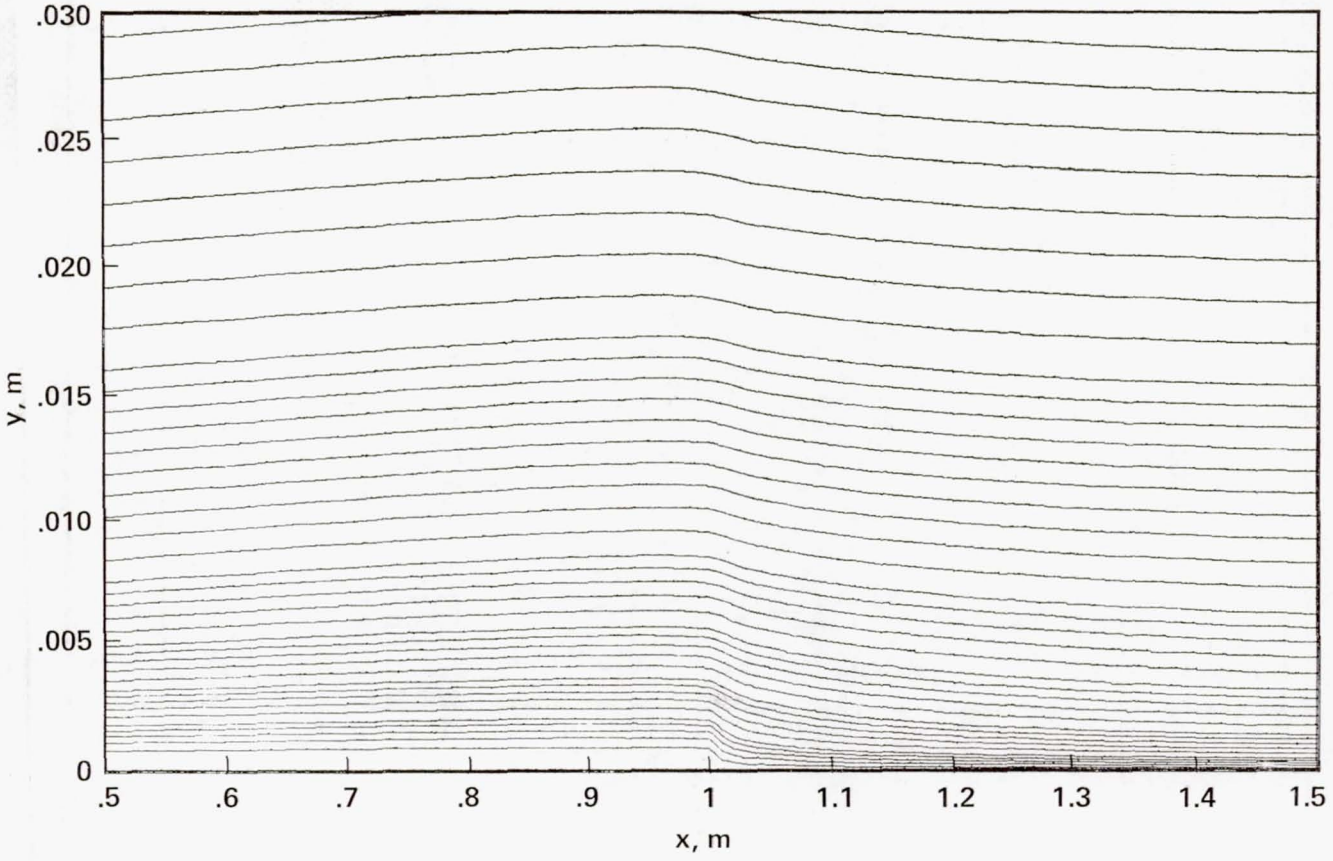

Figure 16. – Streamline contours for trailing-edge interaction: BL-Direct with PNS wall pressures.

1. Report No.	2. Government Accession No.	3. Recipient's Catalog No.
NASA TM-84378		

4. Title and Subtitle	5. Report Date
PARABOLIZED NAVIER-STOKES SOLUTIONS OF SEPARATION AND TRAILING-EDGE FLOWS	June 1983
	6. Performing Organization Code

7. Author(s)	8. Performing Organization Report No.
James L. Brown	A-9394
	10. Work Unit No. T-4219
9. Performing Organization Name and Address	11. Contract or Grant No.
NASA Ames Research Center Moffett Field, Calif. 94035	
	13. Type of Report and Period Covered
12. Sponsoring Agency Name and Address	Technical Memorandum
National Aeronautics and Space Administration Washington, D.C. 20546	14. Sponsoring Agency Code 506-51-11-04-00

15. Supplementary Notes

Point of Contact: James L. Brown, Ames Research Center, MS 229-1, Moffett Field, Calif. 94035. (415) 965-6192 or FTS 448-6192.

16. Abstract

A robust, iterative solution procedure is presented for the parabolized Navier-Stokes or higher-order boundary-layer equations as applied to subsonic viscous-inviscid interaction flows. The robustness of the present procedure is due, in part, to an improved algorithmic formulation. The present formulation is based on a reinterpretation of stability requirements for this class of algorithms and requires only second-order-accurate backward or central differences for all streamwise derivatives. Upstream influence is provided for through the algorithmic formulation and iterative sweeps in x. The primary contribution to robustness, however, is the boundary-condition treatment, which imposes global constraints to control the convergence path. Discussed are successful calculations of subsonic, strong viscous-inviscid interactions, including separation. These results are consistent with Navier-Stokes solutions and triple-deck theory.

17. Key Words (Suggested by Author(s))	18. Distribution Statement
Separation Trailing-edge flows Viscous-inviscid interaction Parabolized Navier-Stokes	Unlimited Subject Category: 34

19. Security Classif. (of this report)	20. Security Classif. (of this page)	21. No. of Pages	22. Price*
Unclassified	Unclassified	49	A03

*For sale by the National Technical Information Service, Springfield, Virginia 22161